

1 **Using beryllium-7 to assess cross-tropopause**
2 **transport in global models**

3
4 Hongyu Liu¹, David B. Considine², Larry W. Horowitz³, James H. Crawford², Susan E.
5 Strahan^{4,5}, Megan R. Damon⁵, Jose M. Rodriguez⁵, Xiaojing Xu⁶, Claire Carouge⁷, and Robert
6 M. Yantosca⁷

7 ¹National Institute of Aerospace, Hampton, VA

8 ²NASA Langley Research Center, Hampton, VA

9 ³NOAA Geophysical Fluid and Dynamics Laboratory, Princeton, NJ

10 ⁴University of Maryland, Baltimore County, MD

11 ⁵NASA Goddard Space Flight Center, Greenbelt, MD

12 ⁶Scientific Systems and Applications, Inc., Hampton, VA

13 ⁷Harvard University, Cambridge, MA

14
15 **Short Title:** Beryllium-7 and cross-tropopause transport

16 **Index Terms:** 0368 Troposphere: constituent transport and chemistry; 3362
17 Stratosphere/troposphere interactions; 3337 Global climate models; 3315 Data assimilation.

18 **Keywords:** stratosphere-troposphere exchange (STE), radionuclide aerosol tracers, wet
19 scavenging, global climate models, assimilated meteorology, Global Modeling Initiative (GMI),
20 3-D chemistry transport model (CTM)

21
22 *JGR -Atmospheres*, submitted, August 2010

23
24 **Correspondence:** Hongyu Liu

25 Mail Stop 401B, NASA Langley Research Center

26 Hampton, VA 23681

27 Tel: 757-864-3191; Fax: 757-864-6326; Email: hyl@nianet.org

28

29 **Abstract.** We assess within the Global Modeling Initiative (GMI) modeling framework the
30 utility of cosmogenic beryllium-7 (^7Be), a natural aerosol tracer, for evaluating cross-tropopause
31 transport in global models. The GMI chemical transport model (CTM) was used to simulate
32 atmospheric ^7Be distributions using four different meteorological data sets (GEOS1-STRAT
33 DAS, GISS II' GCM, fvGCM, and GEOS-4 DAS), featuring significantly different stratosphere-
34 troposphere exchange (STE) characteristics. The simulations were compared with the upper
35 troposphere / lower stratosphere (UT/LS) ^7Be climatology constructed from ~25 years of aircraft
36 and balloon data, as well as climatological records of surface concentrations and deposition
37 fluxes. Comparison of the fraction of surface air of stratospheric origin estimated from the ^7Be
38 simulations with observationally-derived estimates (i.e., 23-27% of the annual mean ^7Be in
39 surface air at northern mid-latitudes originates from the stratosphere [Dutkiewicz and Husain,
40 1985, referred to as DH85]) indicates excessive cross-tropopause transport at middle latitudes in
41 simulations using GEOS1-STRAT and at high latitudes using GISS II' meteorological data.
42 These simulations also overestimate ^7Be deposition fluxes at middle latitudes (GEOS1-STRAT)
43 and at high latitudes (GISS II'), respectively. We show that excessive cross-tropopause transport
44 of ^7Be corresponds to overestimated stratospheric contribution to tropospheric ozone. Our
45 perspectives on STE in these meteorological fields based on ^7Be simulations are consistent with
46 previous studies with the same meteorological fields using ozone as a tracer for STE. We further
47 applied the DH85 constraint to other global models including GFDL AM2 and GEOS-Chem
48 (driven by GEOS-3 DAS and GEOS-5 DAS). We conclude that the DH85 constraint for ^7Be and
49 observed ^7Be total deposition fluxes can be used routinely as a first-order assessment of cross-
50 tropopause transport in global models.

51

52 **1. Introduction**

53 Stratosphere-troposphere exchange (STE) of air masses and chemical species occurs at
54 small-, synoptic and global-scales. It is typically associated with the occurrences of tropopause
55 folding and cutoff cyclones and, more important, the global circulation of the atmosphere
56 [Holton *et al.*, 1995]. While stratosphere-to-troposphere transport removes many chemical
57 species from the stratosphere, it represents a significant source of ozone and other reactive
58 species for the tropospheric chemical system [Stohl *et al.*, 2003]. Ozone in the troposphere is an
59 important greenhouse gas, especially in the upper troposphere. It is a harmful pollutant near the
60 surface. It is also the main precursor of hydroxyl radicals (OH) and thus plays an essential role in
61 the oxidizing capacity of the troposphere. In a warmer climate, the stratosphere is likely to
62 increase its contribution to tropospheric ozone levels due to circulation changes [Collin *et al.*,
63 2003]. Quantitative understanding and prediction of anthropogenic (versus natural) perturbations
64 to tropospheric ozone require the use of global 3-D models; correctly representing the STE flux
65 in these models is therefore critical. However, current models show large (30%) uncertainty in
66 predicted STE fluxes of ozone [Stevenson *et al.*, 2006]. We use here the Global Modeling
67 Initiative (GMI) modeling framework [Douglass, *et al.*, 1999; Rotman *et al.*, 2001] to assess the
68 utility of the aerosol tracer beryllium-7 (^7Be) for evaluating cross-tropopause transport in global
69 models.

70 Beryllium-7 (half-life 53.3 days) is produced by cosmic ray spallation reactions in the
71 stratosphere and upper troposphere. After production, it attaches immediately to available
72 submicron aerosols. The fate of ^7Be then becomes that of those aerosols, which move with the air
73 until scavenged by precipitation or deposited to the surface. With wet deposition as its principal
74 sink and relatively well known sources, ^7Be is a useful aerosol tracer for testing wet deposition

75 processes in a global 3-D model and is often used in pair with the terrigenous ^{210}Pb aerosol tracer
76 [e.g., Brost et al., 1991; Koch et al., 1996; Liu et al., 2001]. On the other hand, because of its
77 source at high altitudes and the large concentration vertical gradient, simulation of ^7Be tests the
78 model's capability to describe stratosphere-to-troposphere transport and subsidence in the
79 troposphere [e.g., Liu et al., 2001; Allen et al., 2003].

80 Beryllium-7 has long been recognized as a tracer of downward transport from the
81 stratosphere to the troposphere [e.g., Husain et al., 1977; Viezee and Singh, 1980; Sanak et al.,
82 1985; Dibb et al., 1992, 1994; Rehfeld and Heimann, 1995]. Husain et al. [1977] reported that
83 pulses of high ^7Be concentrations were often associated with air masses of stratospheric origin,
84 as indicated by large potential vorticities. Viezee and Singh [1980] showed that the ^7Be
85 concentrations over North America show strong positive correlations with the occurrence of
86 tropopause folding events over several latitude belts. ^7Be has also been combined with other
87 radionuclides (e.g., ^{10}Be , ^{90}Sr) as an indicator of transport of stratospheric air to the troposphere
88 [Raisbeck et al., 1981; Rehfeld and Heimann, 1995; Koch et al., 1998; Dibb et al., 1994; Jordan
89 et al., 2003; Zanis et al., 2003; Heikkila et al., 2008ab]. Dutkiewicz and Husain [1985, hereafter
90 referred to as DH85] analyzed ^7Be and ^{90}Sr concentrations measured simultaneously in samples
91 from NASA's Global Atmospheric Sampling Program (GASP) and showed that on an annual
92 basis the stratosphere contributed ~25% of the observed ^7Be concentration at the surface (~40%
93 during late spring but only 10% during fall).

94 Beryllium-7 is also a useful tracer for vertical mixing and subsidence in the troposphere.
95 Feely et al. [1989] examined the factors that contribute to seasonal variations in ^7Be
96 concentrations in surface air. They found that the influences of variations both in the STE rate
97 and in the tropospheric vertical mixing rate are evident in concentrations at most sites in middle

98 latitudes. Convective transport carries surface air upward and brings down to the surface layer
99 the ^7Be at higher altitudes. This is also reflected by the $^7\text{Be}/^{210}\text{Pb}$ ratio that peaks at the surface in
100 summer when convective activity is maximum [Koch et al., 1996]. On the other hand, despite
101 the UT/LS source of ^7Be and the continental surface source of ^{222}Rn (precursor of ^{210}Pb), ^7Be
102 concentrations have been reported to be positively correlated with ^{210}Pb concentrations,
103 reflecting mixing of subsiding middle- and upper-tropospheric air with continental lower-
104 tropospheric air [Li et al., 2002; Dibb, 2007].

105 A number of observational studies have demonstrated the feasibility of using ^7Be to infer
106 the contribution of ozone-rich stratospheric air to ozone levels at ground level [e.g., Husain et al.,
107 1977; Tsutsumi et al., 1998; Helmig et al., 2007] and in the free troposphere [e.g., Johnson and
108 Viezee, 1981; Prospero et al., 1995; Graustein and Turekian, 1996; Kritz et al., 1991; Dibb et al.,
109 2003]. These studies are usually based on the correlations between concurrent measurements of
110 ozone and ^7Be (as well as other tracers such as water vapor and potential vorticity), with positive
111 ^7Be -ozone correlations indicating the presence of the upper-tropospheric or stratospheric air. For
112 instance, Helmig et al. [2007] showed a year-round correlation of ozone with ^7Be at Summit,
113 Greenland and concluded that surface-layer photochemical ozone production does not appear to
114 have a noticeable influence on surface ozone levels. It is important to note, however, that under
115 some circumstances the observed positive correlations of surface ozone with ^7Be may simply
116 reflect the common vertical trends of tropospheric ^7Be and ozone and does not necessarily
117 indicate the influence of stratospheric air [Li et al., 2002]. Recent global modeling studies
118 showed the models' capability to reproduce the observed ^7Be -ozone relationships, providing
119 useful constraints on the stratospheric (versus photochemical) contribution to tropospheric ozone
120 in the model [Li et al., 2002; Allen et al., 2003; Liu et al. [2004].

121 Though correct representation of STE is essential for simulating ^7Be , ozone and other trace
122 species in the troposphere, large variations exist among models. Stevenson et al. [2006] reported
123 the average STE flux of ozone from 26 models of 552 ± 168 Tg/year, while the IPCC Third
124 Assessment Report (TAR) [Prather and Ehhalt, 2001] reported a mean value of 770 Tg/year.
125 However, observation-based estimates of STE fluxes of ozone into the troposphere are typically
126 in the range of 400-600 Tg/year [Murphy and Fahey, 1994]. Some global models are able to
127 produce STE fluxes of ozone in this range [e.g., Olsen et al., 2004; Hsu et al., 2005; Hsu and
128 Prther, 2009]. For those models with too fast (or rarely, too slow) cross-tropopause transport of
129 ozone, one way to overcome the difficulty is to use the Synoz (synthetic ozone) method
130 [McLinden et al., 2000]. The Synoz method involves constraining the global mean cross-
131 tropopause ozone flux to match a prescribed value consistent with observations [e.g., Bey et al.,
132 2001]. But this method yields unrealistic stratospheric ozone field and therefore does not allow
133 for on-line calculations of total ozone columns and photolysis rates / heating rates [McLinden et
134 al.,2000]. By contrast, the other simple model for stratospheric ozone (linearized ozone or Linoz)
135 developed by McLinden et al. enables these on-line calculations by linearizing the ozone
136 tendency about the local ozone mixing ratio, temperature, and the overhead column ozone
137 density. Linoz is computationally efficient and can be readily incorporated in climate models for
138 long-term integrations. Nevertheless, using Linoz (or full stratospheric chemistry) in global
139 CTMs or chemistry-climate models that focus on the troposphere requires a reasonable model
140 representation of cross-tropopause transport. In this context, ^7Be tracer simulations may provide
141 a simple way of evaluating cross-tropopause transport in these models.

142 The intermodel differences in the estimated intensity and frequency of STE have been
143 attributed to the different meteorological fields used to drive the models as well as different

144 descriptions of transport and chemistry processes [Cristofanelli et al. 2003]. The GMI modeling
145 framework facilitates the reduction of uncertainties of this kind. It is a modular CTM with the
146 ability to incorporate different inputs and components (e.g., meteorological fields, emission
147 inventories, chemical and microphysical mechanisms, and numerical schemes) that represent the
148 different approaches of current models. One of the distinct features of the GMI CTM is the
149 ability to be driven with several sets of meteorological data [e.g., Douglass et al., 1999;
150 Considine et al., 2005; Liu et al., 2007]. This allows us to isolate the uncertainties in the model
151 simulations due to differences in the meteorological data sets alone. The number of factors that
152 may contribute to differences in the simulations is thus reduced, as we previously showed using
153 the GMI simulated ^{222}Rn and ^{210}Pb radionuclide tracers [Considine et al., 2005].

154 In this paper, we present simulations of atmospheric ^7Be distributions with the GMI CTM
155 driven by four different meteorological data sets, including output from GEOS1-STRAT, GISS
156 II' GCM, fvGCM, and GEOS4-DAS, featuring significantly different STE characteristics. We
157 use here not only the meteorological fields that are well known to have reasonably good
158 representations of STE (e.g., fvGCM) but also those with incorrect representations (e.g., GEOS1-
159 STRAT). The variability in the model performances of representing STE allows us to examine
160 and assess the utility of ^7Be for evaluating STE in these (and other) global meteorological fields.
161 We will illustrate the consequences of incorrect STE in terms of the simulation of tropospheric
162 ^7Be and show that ^7Be concentrations and deposition fluxes may be used routinely to assess
163 cross-tropopause transport in global models. We will discuss how the constraints on STE from
164 ^7Be are consistent with previous modeling studies of tropospheric ozone using the same
165 meteorological fields. We will also apply the ^7Be tracer to assess cross-tropopause transport in
166 GFDL AM2 GCM and in other meteorological fields (GEOS-3 DAS and GEOS-5 DAS).

167 The balance of this paper is organized as follows. Section 2 gives a brief description of the
168 GMI model, ^7Be source and cross-tropopause flux, and ^7Be and ozone observational datasets
169 used for evaluating the model. Section 3 evaluates model results with UT/LS and surface ^7Be
170 data. Section 4 assesses cross-tropopause transport of ^7Be in different meteorological fields.
171 Section 5 compares the results with previous modeling studies. Section 6 assesses cross-
172 tropopause transport of ^7Be in a few other meteorological fields. Section 7 discusses the
173 implications for the impact of STE on tropospheric ozone, followed by summary and conclusions
174 in section 8.

175

176 **2. Model and Data**

177 **2.1. GMI CTM**

178 The GMI (<http://gmi.gsfc.nasa.gov>) CTM is a global 3-D composition model that includes
179 a nearly full treatment of both stratospheric and tropospheric photochemical and physical
180 processes (the so-called Combo model). Details of the model are described in Duncan et al.
181 [2007, 2008], Strahan et al. [2007] and Considine et al. [2008]. There is also a tropospheric
182 version of the model that include only tropospheric photochemical and physical processes and
183 use the Synoz (synthetic ozone) scheme [McLinden et al., 2000] as a flux upper boundary
184 condition for ozone in the stratosphere. The latter yields a cross-tropopause ozone flux of about
185 530-590 Tg/year [Stevenson et al., 2006]. In this study, we use for ^7Be simulations the basic
186 structure of the Combo model (without photochemical modules), as applied previously by
187 Considine et al. [2005] to model the radionuclides ^{222}Rn and ^{210}Pb . We use both the full Combo
188 version and the tropospheric version of the model for ozone simulations.

189 One of the main differences between simulations presented in this paper was the
190 meteorological data used to drive the model. The four different sets of input meteorological data
191 are: (1). output from the Goddard Space Flight Center Data Assimilation Office (now Global
192 Modeling and Assimilation Office or GMAO) GEOS1-STRAT assimilation (GEOS1-STRAT);
193 (2). output from the Goddard Institute for Space Studies GISS II' general circulation model
194 (GISS II' GCM) [Rind and Lerner, 1996]; (3). the GMAO finite-volume GCM (fvGCM); and
195 (4). output from the GMAO GEOS-4 data assimilation system (GEOS-4 DAS). Vertical levels,
196 top pressure, original / run resolutions, near-tropopause resolution, and bottom layer depth are
197 listed in **Table 1**. The simulations presented here use a degraded horizontal resolution ($4^{\circ}\times 5^{\circ}$) for
198 computational expediency. Degraded horizontal resolution has some consequences for the
199 simulation of cross-tropopause transport [Liu et al., 2001]. Nevertheless, our objective is to
200 assess cross-tropopause transport in meteorological data sets at the resolution used to drive the
201 model, not necessarily at the original or finer resolution.

202 The model uses the flux-form semi-Lagrangian advection scheme and a convective
203 transport algorithm adapted from the CONVTRAN routine in the NCAR CCM3 physics
204 package. The wet deposition scheme is that of Liu et al. [2001] and includes scavenging in wet
205 convective updrafts, and first-order rainout and washout from both convective anvils and large-
206 scale precipitation. The gravitational settling effect of cloud ice particles included in Liu et al.
207 [2001] is not considered here. Dry deposition of ^7Be aerosols is computed using the resistance-
208 in-series approach. For ^7Be simulations, each simulation was run for six years, recycling the
209 meteorological data for each year of the simulation; we use the sixth year output for analysis. For
210 ozone simulations, the model was spun up for 10 years to remove the effect of initial conditions.
211 Interannual variability in STE of ^7Be is not shown in this paper. However, model simulations

212 driven by multi-year output from fvGCM (1994-1998) indicate that such interannual variability
213 is much smaller than the differences due to using different meteorological data sets and does not
214 affect the conclusions of this study.

215 The GMI CTM has been used previously to study the sensitivities of model simulations to
216 different sets of meteorological input. Douglass et al. [1999] used chemical tracers in the GMI
217 framework to assess three meteorological data sets, i.e., the NCAR Community Climate Model
218 (CCM2), GEOS1-STRAT, and GISS II' GCM. They concluded that overall CCM2 provides the
219 best representation of the stratosphere. Considine et al. [2005] used the GMI model to simulate
220 the radionuclides ^{222}Rn and ^{210}Pb using three different sets of meteorological inputs (GEOS1-
221 STRAT, GISS II', and CCM3) and to characterize the variability occurring in their simulations.
222 Overall no simulation was found to be superior to the others when compared with the
223 climatological observations. The role played by convective transport and scavenging was found
224 to differ substantially among the three meteorological data sets. Liu et al. [2007] analyzed and
225 quantified the differences and uncertainties in GMI aerosol simulations solely due to different
226 meteorological fields (GEOS1-STRAT, fvGCM, and GEOS-4 DAS). They suggested that the
227 differences in the precipitation, convective mass flux, and horizontal advection from the three
228 meteorological data sets explain much of the large discrepancies in the model calculated aerosol
229 concentrations.

230 **2.2. ^7Be Source**

231 There is a large discrepancy in the published estimates of ^7Be production rates [Lal and
232 Peters, 1967; O'Brien et al., 1991; Masarik and Reedy, 1995; Masarik and Beer, 1999; Usoskin
233 and Kovaltsov, 2008]. Global mean column production rates over an average solar cycle are
234 $0.035 \text{ atoms cm}^{-2} \text{ s}^{-1}$ [Masarik and Beer, 1999], $0.063 \text{ atoms cm}^{-2} \text{ s}^{-1}$ [O'Brien et al., 1991], and

235 0.081 atoms cm⁻² s⁻¹ [LP67]. The Masarik and Beer [1999] production function is smaller than
236 other estimates by a factor of 2 or more. It may have underestimated the rate of ⁷Be production
237 and slightly overestimated changes in the production rate due to variations in geomagnetic and
238 solar magnetic field strength [Koch et al., 2006; Field et al., 2006]. The rates of ⁷Be production
239 recently reported by Usoskin and Kovaltsov [2008] broadly agree with those of Lal and Peters
240 [1967] with slightly (about 25%) lower global production rate. We use in the model the Lal and
241 Peters [1967] source for 1958 (solar maximum year). About 2/3 of atmospheric ⁷Be is generated
242 in the stratosphere and 1/3 in the troposphere. The ⁷Be production rate correlates inversely with
243 solar activity. At higher solar activity, cosmic rays are deflected away from the solar system and
244 the ⁷Be production rate is thus lower.

245 **2.3. Dutkiewicz and Husain Constraint on ⁷Be Cross-Tropopause Transport**

246 Cross-tropopause transport is important for simulating ⁷Be in the troposphere. A useful
247 constraint on the stratospheric contribution to tropospheric ⁷Be is DH85's analysis of the
248 observed ⁷Be/⁹⁰Sr ratio in the stratosphere and ⁹⁰Sr concentrations at the surface. The presence of
249 fissiogenic ⁹⁰Sr in the troposphere is due entirely to downward transport from the stratosphere,
250 except for a few weeks right after a nuclear detonation. Both ⁷Be and ⁹⁰Sr are associated with
251 submicron particles; their fates during transport from the stratosphere are expected to be similar
252 (no differential removal is expected). The stratospheric ⁷Be component in surface air can
253 therefore be determined as the product of the stratospheric ⁷Be/⁹⁰Sr ratio and the surface ⁹⁰Sr
254 concentration [DH85]. By this procedure, DH85 showed that annually 23-27% (or about 25% on
255 average) of the ⁷Be in surface air at northern midlatitudes is of stratospheric origin. To use this
256 constraint, we diagnose stratospheric contribution to ⁷Be concentrations in the troposphere by
257 transporting separately in the model the ⁷Be produced in the stratosphere, as we previously

258 applied in GEOS-Chem with GEOS1-DAS meteorological data [Liu et al., 2001]. Since wet
259 deposition removes both the stratospheric and tropospheric components of ^7Be at the same rate,
260 the diagnosed stratospheric fraction of ^7Be concentrations in the troposphere does not
261 significantly depend on the rate of wet removal.

262 Downward transport from the stratosphere to troposphere occurs on a time scale of $\sim 1\text{-}2$
263 years. As a result, ^7Be concentrations in the stratosphere are mainly determined by a balance
264 between production and radioactive decay (half-life 53.3 days). On the other hand, ^7Be cross-
265 tropopause transport fluxes are proportional to the downward transport efficiency and ^7Be
266 concentrations in the stratosphere. Therefore, for the simulation of tropospheric (not
267 stratospheric) ^7Be , stratospheric influx to the troposphere may be adjusted by artificially scaling
268 down (in the case of excessive STE) or up (in the case of too slow STE) the stratospheric ^7Be
269 source. The extent to which ^7Be cross-tropopause transport is excessive or too slow in the model
270 can be indicated by a scaling factor A , which is defined as the ratio of model to observation-
271 based STE fluxes of ^7Be . We derive the scaling factor A as follows.

272 According to the Dutkiewicz and Husain [1985] observational constraint, annually the ratio
273 of the tropospheric ($[\text{}^7\text{Be}]_{\text{T}}$) to stratospheric ($[\text{}^7\text{Be}]_{\text{S}}$) component of ^7Be concentrations in surface
274 air at NH mid-latitudes is

$$275 \quad [\text{}^7\text{Be}]_{\text{T}} / [\text{}^7\text{Be}]_{\text{S}} = (1-0.25)/0.25. \quad (1)$$

276 For a global model with its own STE characteristics, we have

$$277 \quad [\text{}^7\text{Be}]_{\text{T}} / [\text{}^7\text{Be}]_{\text{S}'} = (1-F)/F. \quad (2)$$

278 where $[\text{}^7\text{Be}]_{\text{S}'}$ is the model stratospheric component of annual mean ^7Be concentrations in
279 surface air at NH mid-latitudes and F is the corresponding fraction of surface air of stratospheric
280 origin. As the total sink (dry / wet deposition and radioactive decay) is proportional to the

281 amount of ^7Be present, the stratospheric component of ^7Be concentrations in tropospheric air is
282 proportional to stratospheric influx of ^7Be . Thus, we may obtain the scaling factor A by taking
283 the ratio of (1) and (2). That is,

$$284 \quad A = \frac{[^7\text{Be}]_s'}{[^7\text{Be}]_s} = (1-0.25)/0.25 \cdot F/(1-F). \quad (3)$$

285 Unless otherwise specified, ^7Be cross-tropopause fluxes in the model calculations presented in
286 this paper are not adjusted. However, we will use the scaling factor A as one of the metrics for
287 comparing the STE characteristics of different meteorological data sets.

288 **2.4. ^7Be and ozone observational data**

289 **^7Be** We estimate an average solar year value simply by averaging the long-term records of
290 ^7Be observations. We then multiply by 0.72 to correct to the 1958 solar maximum source [Koch
291 et al., 1996]. The ^7Be deposition flux observations are from the compilation of Koch et al. [1996]
292 and there are about 25 northern midlatitude sites from which long-term records of ^7Be
293 observations are available. The ^7Be surface concentration observations are from the data archive
294 of the US Department of Energy (DOE) Environmental Measurements Laboratory (EML, now
295 part of the Department of Homeland Security) Surface Air Sampling Program (SASP) beginning
296 in the 1980's. We also use the long-term climatological data of ^7Be concentrations in the UT/LS
297 constructed from ~25 years of aircraft and balloon observations. Between the late 1950s and the
298 early 1980s, EML collected tropospheric and stratospheric aircraft and balloon measurements of
299 numerous radionuclides as part of the DOE High Altitude Sampling Program (HASP). The data
300 was compiled into a database in 1997 by R. Leifer and N. Chan of EML, the so-called
301 RADioNuclide DATAbase (RANDAB). The reader is referred to Considine et al. [2005] for a
302 brief description of the RANDAB database. This database is available at the Oak Ridge National

303 laboratory's Carbon Dioxide Information Analysis Center
304 (<http://cdiac.esd.ornl.gov/ndps/db1019.html>).

305 **Ozone** We use tropospheric ozone column (TOC) determined with the tropospheric ozone
306 residual method by subtracting measurements of MLS stratospheric column ozone (SCO) from
307 OMI total column ozone [Ziemke et al., 2006; URL: [http://acdb-
308 ext.gsfc.nasa.gov/Data_services/cloud_slice](http://acdb-ext.gsfc.nasa.gov/Data_services/cloud_slice)] or using the TOMS and Solar Backscatter
309 Ultraviolet (SBUV) combination [Fishman et al., 2003; URL: [http://asd-
310 www.larc.nasa.gov/TOR/data.html](http://asd-www.larc.nasa.gov/TOR/data.html)]. We use climatological monthly average ozone profiles
311 from 23 ozonesonde stations as constructed by Considine et al. [2008], based on Logan [1999]
312 and Thompson et al. [2003]. The number of sondes at each station is adequate for defining
313 monthly means used to evaluate the accuracy of the model results [Considine et al., 2008].
314 Surface ozone data are taken from Logan [1999].

315 **3. Model Evaluation With UT/LS and Surface ⁷Be Data**

316 In this section, we present model results of ⁷Be simulations driven by four meteorological
317 archives and evaluate them against long-term measurements at the surface and in the UT/LS. We
318 show in **Figure 1** zonal mean, annual average concentrations of ⁷Be in the four radionuclide
319 simulations with GMI CTM. All four simulations overall show a similar pattern of tropospheric
320 distribution. The highest concentrations are seen in the dry subsiding subtropics. Lowest ⁷Be
321 concentrations in surface air are found in the Southern Hemisphere midlatitudes owing to
322 scavenging by frequent large-scale precipitation. Low ⁷Be concentrations are also associated
323 with ITCZ, which is characterized by strong convergence and convective precipitation. It
324 appears, however, that among all four simulations the GEOS1-STRAT simulation gives the

325 highest concentrations in the subtropics and the GISS simulation shows the highest
326 concentrations in the high latitudes.

327 We compare in **Figure 2** four ^7Be simulations in the upper troposphere / lower stratosphere
328 (UT/LS) with climatological distributions constructed from the ^7Be data contained in the
329 RANDAB database, following Considine et al. [2005] who previously made a similar
330 comparison for ^{210}Pb . Model output are sampled at the months, longitudes, latitudes, and
331 altitudes of the ^7Be observations. **Figure 2a** compares the meridional distribution of ^7Be
332 measurements made in the 12-16km altitude range with the four GMI simulations. **Figure 2b**
333 shows the same comparison, but for the 16-20km altitude range. The 12-16km (about 200-
334 100hPa) range lies within the upper troposphere in the tropics and the lower stratosphere at mid
335 to high latitudes. The 16-20km (about 100-50hPa) range lies within the stratosphere at all
336 latitudes.

337 At 12-16km (**Figure 2a**), the observations indicate comparatively low tropical upper
338 tropospheric values of $\sim 35 \text{ mBq SCM}^{-1}$, with increasing trends toward high latitudes. The
339 distribution is nearly symmetric about the equator, with more observations available in NH high
340 latitudes. This latitudinal distribution of ^7Be concentrations reflects larger production of ^7Be in
341 the lower stratosphere at high latitudes and precipitation scavenging associated with deep
342 convection in the tropics. All four simulations capture reasonably well the observations at 12-16
343 km. The differences between the four simulated ^7Be concentrations are comparable or smaller
344 than the error limits.

345 At 16-20km (**Figure 2b**), the observations show a tropical minimum of $\sim 150 \text{ mBq SCM}^{-1}$,
346 with increasing concentrations toward high latitudes in both hemispheres. In the tropics and the
347 SH, the four ^7Be simulations indicate small differences. In the NH, the four ^7Be simulations

348 reveal large differences and bracket the observations. In particular, the GMI/GEOS1-STRAT
349 simulation gives the lowest ^7Be concentrations among the four simulations and is lower than the
350 observations. This appears to be due to the markedly overestimated cross-tropopause transport in
351 GEOS1-STRAT, as further discussed below. On the other hand, as we will also discuss later, the
352 fvGCM and GEOS-4 DAS meteorological fields characterize reasonable cross-tropopause
353 transport. In the latter case, stratospheric ^7Be concentrations are primarily determined by a
354 balance between production and radioactive decay in the stratosphere. Therefore the slightly
355 overestimated ^7Be at 16-20km may suggest a slightly overestimated global production rate of
356 ^7Be in the Lal and Peters [1967] source. The Usoskin and Kovaltsov [2008] source, which is
357 about 25% lower than the Lal and Peters [1967] source, would probably yield better agreements
358 with the ^7Be observations in the lower stratosphere.

359 **Figure 3a** compares the simulated and observed annual average concentrations of ^7Be near
360 the surface as a function of latitude. Observed data are from the EML SASP database and are
361 averaged into 10 latitude bins. Observations from sites with elevation higher than 500m are not
362 included because of uncertainties involved in sampling coarse-resolution models at high
363 elevation sites. Model results are sampled at observation locations and month. The observations
364 indicate concentration maxima in the subtropics associated with subsidence and minima in the
365 tropics. The tropical minimum reflects rapid scavenging within the ITCZ. Low ^7Be
366 concentrations are also observed at midlatitudes due to efficient scavenging in the midlatitude
367 storm tracks. Latitudinal trends (i.e., minima and maxima) of ^7Be concentrations are well
368 simulated with all meteorological fields except GISS II'. The GMI/GISS simulation shows too
369 high ^7Be concentrations at high latitudes; this is because of the well-known excessive cross-

370 tropopause transport at high latitudes in the GISS II' meteorological fields [e.g., Koch and Rind,
371 1998; McLinden et al., 2000; Shindell et al., 2003].

372 **Figure 3b** compares the model simulated annual mean total deposition fluxes of ^7Be at 25
373 northern midlatitude sites from which long-term records of observations are available. The ^7Be
374 deposition flux observations are from the compilation of Koch et al. [1996] and we previously
375 used this dataset in Liu et al. [2001]. The data from individual sites are averaged over 4° latitude
376 bins. The model is sampled at observation locations. The observations show a maximum (~ 2100
377 $\text{Bq/m}^2/\text{yr}$) in the subtropics ($\sim 30\text{N}$) and the fluxes fall off with increasing latitudes. The four ^7Be
378 simulations show large discrepancies especially in the subtropics ($\sim 30\text{N}$). Overall, the
379 GMI/fvGCM simulation agrees better with the magnitude of the observed fluxes while the
380 GMI/GEOS-4 simulation yields better latitudinal trends. GMI/GEOS-4 simulates best the
381 observations at the latitudes of 45N - 60N , but overestimates the observations by $\sim 50\%$ at 20N -
382 40N . The GMI/GISS simulation overestimates the observations at higher latitudes (45N - 60N) by
383 a factor of ~ 2 . The GMI/GEOS1-STRAT simulation excessively overestimates the observed ^7Be
384 deposition fluxes at subtropical latitudes by up to a factor of 2.5 (30N). We will show in the next
385 section that these overestimated ^7Be deposition fluxes are largely due to model excessive cross-
386 tropopause transport, especially in the GEOS1-STRAT and GISS II' meteorological fields.

387 **4. Assessment of Cross-Tropopause Transport of ^7Be in Different Meteorological Archives**

388 The above results indicate different levels of success with four meteorological archives in
389 reproducing long-term records of surface and UT/LS ^7Be concentrations as well as total
390 deposition fluxes. In this section, we quantify the contribution of ^7Be produced in the
391 stratosphere to tropospheric ^7Be concentrations and deposition fluxes, followed by an assessment
392 of cross-tropopause transport of ^7Be in the meteorological archives used.

393 **Figure 4a** shows the stratospheric fraction (%) of annual zonal mean tropospheric ^7Be
394 concentrations (i.e., fraction of tropospheric ^7Be produced in the stratosphere) in the standard
395 model simulations as a function of latitude and pressure. With GEOS1-STRAT, stratospheric
396 contribution to lower-tropospheric ^7Be concentrations maximizes at 25-50N (35-45%) and 25-
397 40S (30-35%). The tropical middle and upper troposphere shows the minimum in stratospheric
398 impact (<30%). With GISS II', the stratospheric contribution to lower-tropospheric ^7Be
399 concentrations peaks (30-40%) at high latitudes while it is quite small (<~10-20%) in the tropical
400 middle and upper troposphere. The strong gradients in the subtropics suggest that the tropics is
401 strongly isolated from the middle latitudes in the GISS II' meteorological field. fvGCM and
402 GEOS4-DAS show similar pattern of stratospheric influence on the troposphere; both indicate
403 maximum contribution from stratosphere near 30-35N (~25%) and 25-30S (~20-25%) in the
404 lower troposphere. However, GEOS4-DAS shows a few percent larger contributions from the
405 stratosphere to the troposphere than fvGCM does, consistent with the overestimated deposition
406 fluxes at 20N-40N by GEOS4-DAS. The faster STE in GEOS4-DAS is related to the numerical
407 noise introduced by the data assimilation procedures [e.g., Schoeberl et al., 2004]. The area of
408 minimal stratospheric influence in the tropics is also narrower in GEOS4-DAS.

409 **Figure 4b** shows the stratospheric fraction (%) of annual zonal mean surface ^7Be
410 concentrations and ^7Be total deposition fluxes ($\text{Bq}/\text{m}^2/\text{yr}$) in the standard simulation. With all
411 meteorological fields except GISS II', maximum stratospheric contribution to total deposition
412 fluxes (versus surface ^7Be concentrations) is shifted toward higher latitudes, reflecting
413 scavenging by frequent midlatitude precipitation and the dry subsidence in the subtropics.
414 Stratospheric fractions of surface ^7Be concentrations at NH midlatitude are about 38% (GEOS1-
415 STRAT), 33% (GISS II'), and 23-24% (fvGCM and GEOS4-DAS). As discussed in section 2.3,

416 the observed ${}^7\text{Be}/{}^{90}\text{Sr}$ ratio suggests that 23-27% of the ${}^7\text{Be}$ in surface air at northern
417 midlatitudes is of stratospheric origin [Dutkiewicz and Husain, 1985]. According to this
418 constraint, cross-tropopause transport of ${}^7\text{Be}$ and subsequent transport to the surface in the
419 GEOS1-STRAT and GISS II' meteorological fields is excessive. On the other hand, it is
420 noteworthy that the fvGCM and GEOS4-DAS simulations show results remarkably consistent
421 with the DH85 constraint, suggesting that cross-tropopause transport of ${}^7\text{Be}$ in these two
422 meteorological fields are reasonable. However, DH85 did not provide constraints on latitudinal
423 variation of stratospheric influence on surface ${}^7\text{Be}$. Of the four meteorological fields, GEOS1-
424 STRAT, fvGCM and GEOS4-DAS show very similar latitudinal distribution of stratospheric
425 influence at the surface (i.e., peak in the subtropics and valley in the tropics or polar regions). By
426 contrast, GISS II' shows the largest impact of the stratosphere at high latitudes.

427 Similarly, as shown above, the model overestimates the long-term records of ${}^7\text{Be}$
428 deposition flux observations at middle latitudes (and subtropics) with GEOS1-STRAT and at
429 high latitudes with GISS II' (**Figure 3b**). Interestingly, the fvGCM (and to a lesser extent
430 GEOS4-DAS) simulation yields ${}^7\text{Be}$ deposition fluxes close to the observations. This suggests
431 that the DH85 constraint and observed ${}^7\text{Be}$ deposition fluxes are two complementary constraints
432 on cross-tropopause transport of ${}^7\text{Be}$.

433 We therefore use the DH85 constraint to assess the cross-tropopause transport of ${}^7\text{Be}$ in the
434 meteorological fields. Using the approach described in section 2.3 (i.e., reduced cross-tropopause
435 transport flux by artificially scaling down the stratospheric ${}^7\text{Be}$ source in the simulation of
436 tropospheric ${}^7\text{Be}$), we determine the scaling factors for GEOS1-STRAT and GISS to be 1.92 and
437 1.35, respectively. With the adjustment of ${}^7\text{Be}$ cross-tropopause fluxes for GEOS1-STRAT and
438 GISS, the model calculated stratospheric fraction of ${}^7\text{Be}$ concentrations in surface air at NH

439 midlatitudes are indeed close to 25% (i.e., agree with the DH85 constraint) (**Figure 5** vs. **Figure**
440 **4**), thus supporting the validity of equation (3). With the adjustment, the model also simulates
441 better surface ^7Be concentrations and total deposition fluxes at the subtropics (GEOS1-STRAT)
442 and at high latitudes (GISS II') (**Figure 6** vs. **Figure 3**). The improvement is more obvious for
443 total deposition fluxes than for surface concentrations. Total deposition fluxes are a major sink
444 component that largely balances with STE fluxes of ^7Be to the troposphere (source), while
445 surface concentrations are principally dependent on the overall wet removal rate.

446 The above results may be sensitive to the model diagnosed location of tropopause; there is
447 some uncertainty associated with the latter. For instance, Stajner et al. [2008] used four different
448 definitions of the tropopause on the basis of temperature lapse rate (WMO definition), potential
449 vorticity (PV), and isentropic surfaces or ozone isosurfaces. They found that the WMO
450 tropopause was about 0.7-1 km (in the northern midlatitude) or 0.5-1 km (in the tropics) higher
451 than the ozone or PV determined tropopause. We examine here the sensitivity of model
452 diagnosed stratospheric fraction of tropospheric ^7Be concentrations to the location of tropopause
453 (not shown) by lowering tropopause height by one model level (approximately 1.2 km, 1.7 km,
454 1.1 km, 1.1 km for GEOS1-STRAT, GISS II', fvGCM and GEOS4-DAS, respectively). Results
455 indicate that stratospheric fractions of surface ^7Be concentrations increase by 5-10%, thus
456 requiring larger adjustments of cross-tropopause transport of ^7Be in the meteorological fields in
457 order to meet the DH85 constraint. This also suggests that using the DH85 constraint requires
458 relatively high vertical resolution near tropopause in the model.

459

460 **5. Comparison with previous modeling studies**

461 In this section we compare the GMI CTM results for cross-tropopause transport of ^7Be with
462 previous modeling studies based on the same or similar meteorological fields.

463 Liu et al. [2001] found that STE flux of ^7Be was overestimated with the GEOS1-STRAT
464 fields in the GEOS-Chem model, consistent with this study using GMI CTM. However, Liu et al.
465 [2001] found that the reduction required to match the DH85 constraint is a factor of 3.5 for the
466 GEOS1-STRAT archive with $4^\circ \times 5^\circ$ resolution, compared to a factor of 2.5 in the present study.
467 The larger reduction in the former reflects the inclusion of ice particle gravitational settling
468 effect, which results in increased transport from the upper to lower troposphere, as well as the
469 model diagnosed tropopause that is lower by one model layer. Interestingly, when specifying
470 ozone concentrations in the lowermost stratosphere (70hPa) and letting the model (GEOS-Chem)
471 transport this ozone as an inert tracer into the troposphere, Bey et al. [2001] found a similar
472 overestimate in an ozone simulation with the GEOS-1 data, as diagnosed by the simulation of
473 tropospheric ozone concentrations at high latitudes in winter where transport from the
474 stratosphere is a major source. This indicates that model's deficiency in cross-tropopause
475 transport as diagnosed using ^7Be tracers has similar consequences for cross-tropopause transport
476 of ozone.

477 Koch and Rind [1998] used a 31-layer version of the GISS GCM to simulate ^7Be and ^{10}Be
478 and used tropospheric $^{10}\text{Be}/^7\text{Be}$ as indicator of STE. Based on limited observations, they
479 suggested that leakage into the troposphere is somewhat excessive in the model, particularly at
480 high latitudes. Using the GISS II' GCM, McLinden et al. [2000] found that a large fraction of the
481 cross-tropopause transport of ozone occurs at the poles which is inconsistent with the current
482 understanding of stratosphere-troposphere exchange, despite that the global stratosphere-
483 troposphere exchange fluxes of ozone compare well with their best estimate of 475 ± 120 Tg/year

484 based on measurements and tracer-tracer correlation. Shindell et al. [2003] presented an updated
485 version of the GISS II' climate model which still overestimates ozone in the middle troposphere
486 at high latitudes, likely reflecting deficiencies in the model's downward transport of stratospheric
487 air. Our conclusions about cross-tropopause transport of ^7Be in GISS II' in this work are
488 consistent with these previous studies. Overestimated STE fluxes of ^7Be (by a factor of 2-3) as
489 diagnosed in GMI/GISS based on the DH85 constraint simply reflect the incorrect latitudinal
490 distribution of cross-tropopause transport, that is, too fast STE at higher latitudes and too slow
491 STE at lower latitudes. The DH85 constraint was only applicable and applied for NH midlatitude
492 surface and thus does not provide constraint on the model global STE flux of ^7Be if the
493 latitudinal distribution of STE is incorrect.

494 The large-scale stratospheric transport (Brewer-Dobson circulation) in fvGCM has been
495 shown to be realistic [Douglass et al., 2003] and mean age of stratospheric air is similar to
496 observations [Strahan and Douglass, 2004; Douglass et al., 2008; Strahan et al., 2009]. This
497 suggests credible cross-tropopause transport of mass and ozone in fvGCM because the large-
498 scale exchange between the stratosphere and troposphere is largely tied to the Brewer-Dobson
499 circulation through the overworld wave driving [Holton et al., 1995; Olsen et al., 2004]. Based
500 on this finding, the meteorological data from fvGCM was used to drive GMI CTM by several
501 authors to study tropospheric ozone. Considine et al. [2008] evaluated near-tropopause ozone
502 distributions with ozonesonde data. Terao et al. [2008] examined the role of variability in the
503 input of stratospheric ozone on the interannual variability of tropospheric ozone in the northern
504 extratropics. Liang et al. [2009] investigated the impact of stratosphere-to-troposphere transport
505 on tropospheric ozone and NO_x chemistry over the Arctic. By contrast, GEOS4-DAS tends to
506 have too strong of a residual circulation, and the age of air is too young as compared to

507 observations [Schoeberl et al., 2003; Schoeberl, 2004; Douglass et al., 2008]. A GMI CTM
508 simulation driven with the GEOS4-DAS meteorological fields showed the model's inadequacy
509 in simulating upper-tropospheric ozone [Liang et al., 2009]. These findings are consistent with
510 what we illustrated in this study from a perspective of ^7Be tracers. That is, GEOS4-DAS features
511 larger impact of STE on the troposphere (especially UT) than fvGCM does, while the latter has
512 more credible cross-tropopause transport as constrained by observed ^7Be deposition fluxes
513 (**Figure 3b**) and the DH85 criterion (**Figure 4**).

514

515 **6. Application to other meteorological fields**

516 In previous sections, we have established ^7Be as a useful utility for testing the cross-
517 tropopause transport in global models. In practical applications, such as the development and
518 evaluations of new global models, the DH85 constraint may be used routinely to assess the cross-
519 tropopause transport. These models can be either online (e.g., GCMs) or offline (e.g., CTMs
520 driven with archived meteorological data). In this section, we illustrate such applications by
521 applying the DH85 constraint to assess cross-tropopause transport of ^7Be in a few other
522 meteorological fields, including those from GFDL AM2, GEOS3-DAS and GEOS5-DAS. Model
523 simulations are conducted with AM2 GCM and GEOS-Chem CTM (driven by a series of GEOS-
524 DAS meteorological data), respectively.

525 The GFDL coupled chemistry-climate model (AM2-Chem) is developed by implementing
526 a tropospheric chemistry package from the global MOZART-2 model [Horowitz et al., 2003]
527 within the AM2 climate model [GFDL GAMDT, 2004]. Built on this framework, we have made
528 the model capable of simulating both ^{210}Pb and ^7Be aerosol tracers by implementing their sources
529 and sinks, i.e., dry and wet deposition, and radioactive decay (Liu et al., Lead-210 and beryllium-

530 7 simulations with the new GFDL global atmosphere model AM2, Technical report, submitted to
531 UCAR Visiting Scientist Program, Boulder, CO, May 2006). The model has a resolution of 2.0°
532 latitude by 2.5° longitude with 24 vertical hybrid levels. In the vertical, sigma surfaces near the
533 surface continuously transform to pressure surfaces above 250 hPa. Nine model layers are
534 located below 1.5 km above the surface. The resolution is approximately 2 km in the upper
535 troposphere. There are five levels in the stratosphere, with top level at about 3 hPa. We use the
536 Lal and Peters [1967] ^7Be source for 1958, and the Harvard wet deposition scheme for the
537 rainout (in-cloud scavenging) and washout (below-cloud scavenging) due to stratiform
538 precipitation [Liu et al., 2001]. Convective scavenging of aerosols was coupled with the RAS
539 cumulus parameterization. We conduct model integrations for six years (1982–1987) forced with
540 observed sea surface temperature and use the year 1987 for analysis. Interannual variability does
541 not significantly affect our results.

542 When the model vertical grid level containing the tropopause is included as part of the
543 troposphere, the AM2-Chem diagnosed stratospheric fraction of surface ^7Be at NH mid-latitudes
544 (~25-30%) qualitatively agrees with the DH85 criterion (**Figure 7**). However, when it is
545 included as part of the stratosphere, the corresponding fraction would dramatically increase to
546 ~45% (not shown), reflecting the very coarse resolution near the tropopause. Thus, ^7Be is a
547 useful diagnostic of cross-tropopause transport only when there is high vertical resolution around
548 the tropopause region, so that the variability associated with its placement is relatively low. Such
549 is the case in the newer version of the AM model (AM3 with 48 vertical levels).

550 We previously assessed the cross-tropopause transport of ^7Be in GEOS1-DAS and GEOS1-
551 STRAT-DAS with the GEOS-Chem model [Liu et al., 2001]. We extend here the assessment to
552 other meteorological fields that drives GEOS-Chem, including GEOS3-DAS (2001), GEOS4-

553 DAS (2004) and GEOS5-DAS (2004). GEOS4-DAS has been assessed earlier for cross-
554 tropopause transport of ^7Be with GMI CTM but is included here for comparison purposes. In
555 particular, GEOS5-DAS is the most recent version of the GEOS series of assimilated
556 meteorological dataset available at NASA GMAO. It is being widely used in tropospheric
557 chemistry modeling studies, for which characterizing cross-tropopause transport in GEOS5-DAS
558 has important implications. **Figure 8** shows stratospheric fraction (%) of annual zonal mean
559 tropospheric ^7Be concentrations as a function of latitude and pressure as simulated by GEOS-
560 Chem driven with GEOS3-DAS, GEOS4-DAS and GEOS5-DAS, respectively. Slower cross-
561 tropopause transport is seen in GEOS3-DAS than in GEOS4-DAS and GEOS5-DAS. This may
562 partly explain the low ^7Be bias in the lower troposphere in a CTM driven with GEOS3-DAS
563 [Allen et al., 2003]. Overall, both the GEOS4-DAS and GEOS5-DAS represent reasonably well
564 the impact of cross-tropopause transport on surface ^7Be concentrations on the basis of the DH85
565 constraint. This shows that models which utilize either of these fields could implement the
566 “Linoz” ozone scheme and expect satisfactory results. However, GEOS-5-DAS shows smaller
567 STE influence in the middle troposphere than GEOS4-DAS and is more consistent with
568 GMI/fvGCM (**Figure 8** vs. **Figure 4a**). As discussed above, fvGCM has more credible cross-
569 tropopause transport than GEOS4-DAS. This suggests that GEOS5-DAS improves over GEOS4-
570 DAS on the impact of cross-tropopause transport on the upper and middle troposphere.

571

572 **7. Implications for cross-tropopause transport of ozone**

573 In this section we discuss the implications of different characteristics of cross-tropopause
574 transport of ^7Be for stratospheric influence on tropospheric ozone in different meteorological
575 fields. At the time of this writing, the GMI Combo model can be driven with GEOS1-STRAT,

576 fvGCM and GEOS4-DAS (not GISS II') meteorological fields. This allows us to examine any
577 potential relationship between the cross-tropopause transport of ^7Be and ozone when these fields
578 are used to drive the model.

579 Ozonesonde, surface and satellite observations provide useful constraints on the
580 stratospheric contribution to tropospheric ozone [e.g., Rind et al., 2007]. **Figure 9** shows
581 comparisons of model tropospheric ozone profiles with annual mean ozonesonde observations
582 for a range of latitudes [Consideine et al., 2008]. These results are typical of other stations at
583 similar latitudes. The GMI/GEOS1-STRAT simulation produces excessive ozone throughout the
584 troposphere at all latitudes except in the tropics while the GMI/fvGCM and GMI/GEOS4-DAS
585 simulations are generally in agreement with the observations (with slightly overpredicted ozone
586 in the midlatitude upper troposphere). The model overestimate with GEOS1-STRAT is largest
587 in spring. We also compared model surface ozone concentrations with the Logan [1999] surface
588 ozone dataset (not shown). Among the three GMI Combo simulations, the GMI/GEOS1-STRAT
589 simulation shows the largest errors in surface ozone concentrations during winter and spring
590 when stratospheric contribution is at its peak. These are in line with the relative magnitudes of
591 cross-tropopause transport efficiencies of ^7Be in the three meteorological fields (i.e., too fast STE
592 in GEOS1-STRAT), which we discussed in previous sections. Indeed, the tropospheric version
593 of the GMI/GEOS1-STRAT model with constrained STE flux of ozone (about 579 Tg/year)
594 simulates ozonesonde observations of tropospheric ozone reasonably well (dotted line, **Figure**
595 **9**).

596 **Figure 10** shows GMI simulated annual zonal mean tropospheric ozone column (TOC), in
597 Dobson Units, compared with observed climatologies (October 2004-July 2008) from
598 TOMS/SBUV [Fishman et al., 2003] and OMI/MLS [Ziemke et al., 2006]. The WMO definition

599 of thermal tropopause is used to calculate the model TOC. While the GMI/fvGCM and
600 GMI/GEOS4-DAS simulations are similar and overestimate the observations by up to ~20 DU,
601 the GMI/GEOS1-STRAT simulation overestimates the observations by as large as ~40 DU. The
602 excessive estimate by GMI/GEOS1-STRAT with maxima at 30°N and 30°S suggests too fast
603 downward transport of ozone from the stratosphere. The tropospheric version of the
604 GMI/GEOS1-STRAT model with constrained STE flux of ozone provides a much better
605 simulation of global TOCs (red dashed line, **Figure 10**), which are comparable to those from
606 GMI/fvGCM and GMI/GEOS4-DAS simulations. However, model TOCs are still ~10-14DU
607 larger than satellite observations in the subtropics and midlatitudes. Previously, *Ziemke et al.*
608 [2006] considered uncertainties in both model and observations and subjectively interpreted
609 model-OMI/MLS TOC differences of 10 DU and higher as significant. As *Stajner et al.* [2008]
610 noted, too low extratropical tropopause used by *Ziemke et al.* [2006] may have played an
611 important role in the underestimation of OMI/MLS TOC. *Yang et al.* [2010] also found that their
612 OMI/MLS potential vorticity mapped TOCs are smaller than ozonesonde TOCs by 5.9 DU with
613 a standard deviation of the differences of 8.4 DU. On the other hand, the GMI/fvGCM
614 simulation tends to overestimate the upper-tropospheric (near-tropopause) ozone at midlatitudes
615 (Figure 9); these biases do not appear to be due to excessive stratospheric influence [*Considine et*
616 *al.*, 2008]. Current global models, including the GMI model, also overpredict surface ozone
617 during summer and early fall over the eastern U.S. and Japan [*Fiore et al.*, 2009]. Therefore the
618 model TOCs are very likely biased high.

619 We further examine the relationship between the cross-tropopause transport of ⁷Be and
620 ozone with the GEOS1-STRAT meteorological fields, in which case STE is known to be too
621 fast. **Figure 11a** shows the latitudinal variations of annual zonal mean tropospheric ⁷Be column

622 overestimate ($\Delta^7\text{Be}$) and TOC overestimate (ΔTOC) in the GMI/GEOS1-STRAT simulation.
623 $\Delta^7\text{Be}$ is obtained by subtraction of the STE-flux-adjusted simulation (section 2.3) from the
624 standard simulation. ΔTOC is obtained by subtraction of the GMI tropospheric model simulation
625 (with STE flux of ozone about 579 Tg/year) from the GMI Combo model simulation. **Figure**
626 **11b** shows the correlation between the global distributions of $\Delta^7\text{Be}$ and ΔTOC . The lines of best
627 fit are calculated using the reduced-major-axis (RMA) method [*Hirsch and Gilroy, 1984*].
628 Standard errors for the intercept and the slope are computed as described by *Miller and Kahn*
629 [1962]. Overall, the location of overestimated ozone follows that of overestimated ^7Be , with both
630 maxima near 30°N and 30°S. The strong correlation between $\Delta^7\text{Be}$ and ΔTOC implies that ^7Be is
631 a good indicator of cross-tropopause transport of ozone. These support our conclusion that ^7Be is
632 a useful utility for assessing cross-tropopause transport of ozone in global models.

633

634 **8. Summary and Conclusions**

635 We have assessed the ability of the Global Modeling Initiative (GMI) chemical transport
636 model (CTM) to simulate the atmospheric distributions of ^7Be , a natural aerosol tracer
637 originating from the upper troposphere/lower stratosphere and removed from the troposphere
638 primarily by wet deposition. The model was driven by four meteorological data sets (GEOS1-
639 STRAT, GISS-II', fvGCM, GEOS-4 DAS) which feature different cross-tropopause transport
640 characteristics. The GMI modeling framework was configured such that the variability between
641 the simulations mainly reflects the use of different meteorological data. Our goal was to assess
642 the utility of ^7Be as a tracer of cross-tropopause transport in global models and develop a
643 methodology to exploit such a utility. We have also discussed the implications of excessive

644 cross-tropopause transport as revealed by ^7Be simulations for the modeling of tropospheric
645 ozone.

646 We evaluated the four simulations of ^7Be with RANDAB, a unique database of upper
647 atmosphere radionuclide climatological observations compiled by the DOE (now DHS)
648 Environmental Measurement Laboratory, as well as long-term measurements at the surface.
649 Model simulations capture well the UT/LS observations with respect to latitudinal distributions.
650 The GMI/GEOS1-STRAT simulation shows the lowest ^7Be concentrations among the four
651 simulations in the lower stratosphere, and underestimates the observations. This reflects the
652 well-known highly overestimated cross-tropopause transport in GEOS1-STRAT DAS. At the
653 surface, the model simulates well the latitudinal trends of ^7Be concentrations, but shows too high
654 ^7Be concentrations at high latitudes in GISS-II'. The GMI/fvGCM simulated ^7Be deposition
655 fluxes are most close to the observations, while the GMI/GEOS1-STRAT overestimates the
656 observed ^7Be deposition fluxes at subtropical latitudes by up to a factor of 2.5 (30°N) and the
657 GMI GISS-II' simulations are too high by factor of 2 at high latitudes (45-60°N). We associated
658 these model performances with the capability of their respective meteorological fields to
659 correctly represent cross-tropopause transport. As such we demonstrated that the observed ^7Be
660 deposition fluxes offer a strong constraint on stratosphere to troposphere transport in global
661 models.

662 We examined within the GMI modeling framework the Dutkiewicz and Husain [1985]
663 (DH85) constraint on the stratospheric contribution to tropospheric ^7Be . DH85 analyzed the
664 observed $^7\text{Be}/^{90}\text{Sr}$ ratio which suggests that 23-27% of the ^7Be in surface air at northern mid-
665 latitudes is of stratospheric origin. This constraint offers a sensitive test of cross-tropopause
666 transport in global models. Comparison of the fraction of surface air of stratospheric origin

667 estimated from the ^7Be simulations with the DH85 constraint indicates excessive cross-
668 tropopause transport at mid-latitudes with the GEOS1-STRAT meteorological fields and at high
669 latitudes with the GISS II' fields. Interestingly, these simulations also overestimate observed ^7Be
670 deposition fluxes at middle and high latitudes, respectively. With a correction to cross-
671 tropopause flux, the model simulates better surface ^7Be concentrations and total deposition
672 fluxes. By contrast, the fvGCM meteorological data yield most reasonable cross-tropopause
673 transport of ^7Be according to the DH85 constraint, consistent with the fact that the GMI/fvGCM
674 simulated ^7Be deposition fluxes are most close to the observations. These results illustrate that
675 the GMI framework is very useful for characterizing and helping reduce uncertainties in the
676 processes such as cross-tropopause transport in the meteorological fields that are used to drive
677 chemical transport models. Note that since wet deposition removes both the stratospheric and
678 tropospheric components of ^7Be nondiscriminatively, the model diagnosed fraction of ^7Be of
679 stratospheric origin does not significantly depend on the rate of wet removal.

680 The model diagnosed stratospheric fraction of ^7Be in surface air is sensitive to the
681 diagnosed location of tropopause, in particular when the model vertical resolution is relatively
682 coarse near the tropopause region. This suggests that stratospheric fraction of ^7Be is a useful
683 diagnostic when the model has sufficient vertical resolution so that the tropopause can be well
684 defined. We used the WMO definition of thermal tropopause and include the diagnosed
685 tropopause model layer as part of the troposphere (versus the stratosphere). As such our
686 assessment of cross-tropopause transport of ^7Be in the four meteorological data sets (GEOS1-
687 STRAT, GISS II', fvGCM, and GEOS4-DAS) are consistent with previous modeling studies of
688 stratospheric influence on tropospheric ozone with the same meteorological data sets.

689 We further applied the DH85 constraint to assess cross-tropopause transport of ^7Be in other
690 meteorological data sets, including those from GFDL AM2 GCM (via online simulation),
691 GEOS-3 DAS and GEOS-5 DAS (via offline GEOS-Chem model simulation). The diagnosed
692 stratospheric fraction of surface ^7Be at NH mid-latitudes in AM2 qualitatively agrees with the
693 DH85 constraint. However, this diagnostic has a large uncertainty due to the coarse resolution
694 near the tropopause region in AM2. Slower cross-tropopause transport is seen in GEOS3-DAS
695 than in GEOS4-DAS and GEOS5-DAS; the latter two meteorological fields represent the impact
696 of cross-tropopause transport on surface ^7Be concentrations reasonably well. One of the
697 implications is that it would be appropriate to implement “Linoz” ozone [McLinden et al., 2000]
698 in a chemical transport model driven with GEOS-4 DAS or GEOS-5 DAS. On the other hand,
699 similar to fvGCM, GEOS5-DAS appears to show a smaller impact of cross-tropopause transport
700 on the upper and middle troposphere, improving over GEOS-4 DAS.

701 Incorrect cross-tropopause transport of ^7Be implies misrepresented downward influx of
702 stratospheric ozone to the troposphere in a model. We demonstrated this by examining the
703 relationship between the cross-tropopause transport of ^7Be and ozone as simulated by GMI CTM
704 driven with GEOS1-STRAT, fvGCM and GEOS4-DAS meteorological fields. We found that
705 excessive cross-tropopause transport of ^7Be corresponds to overestimated stratospheric
706 contribution to tropospheric ozone, as constrained by ozonesonde, surface and satellite
707 observations.

708 In summary, the ^7Be simulation, which is computationally cheap and technically simple, in
709 combination with the DH85 ^7Be observational constraint and observed ^7Be deposition fluxes
710 may be used routinely to assess cross-tropopause transport in global models. We recommend
711 transporting separately in the model the ^7Be produced in the stratosphere (^7Be -strat) and

712 evaluating the ratio of ^7Be -strat to total ^7Be (i.e., beryllium-7 produced in both the stratosphere
713 and the troposphere) in surface air against the DH85 constraint, as illustrated in this paper. This
714 can serve as a first-order assessment of cross-tropopause transport in the model and therefore
715 help determine whether either “Synoz” or “Linoz” ozone should be used for the stratosphere in
716 the studies that focus on the troposphere. While this study uses ^7Be alone, future work will
717 include using $^{10}\text{Be}/^7\text{Be}$, a more sensitive indicator of STE [Rehfeld and Heimann, 1995; Koch et
718 al., 1998; Jordan et al., 2003], within the GMI modeling framework.

719

720 **Acknowledgments.** This work was supported by the NASA Modeling, Analysis and Prediction
721 (MAP) program and partly by NOAA GFDL. We thank Bryan Duncan and Steve Steenrod for
722 their contributions to the GMI model development. The GMI core team at NASA GSFC is
723 acknowledged for programming support. NASA Center for Computational Sciences (NCCS) and
724 GFDL provided supercomputing resources. The GEOS-Chem model is managed by the
725 Atmospheric Chemistry Modeling Group at Harvard University with support from the NASA
726 Atmospheric Chemistry Modeling and Analysis Program (ACMAP).

727

728 **References**

729

730 Allen, D. J., J. E. Dibb, B. Ridley, K. E. Pickering, and R. W. Talbot (2003), An estimate of the
731 stratospheric contribution to springtime tropospheric ozone maxima using TOPSE
732 measurements and beryllium-7 simulations, *J. Geophys. Res.*, *108*(D4), 8355,
733 doi:10.1029/2001JD001428.

734 Arimoto, R., et al. (1999), Influences of atmospheric transport pathways on radionuclide
735 activities in aerosol particles from over the North Atlantic, *J. Geophys. Res.*, *104*, 21,301-
736 21,316.

737 Balkanski, Y.J., D.J. Jacob, and G.M. Gardner (1993), Transport and residence times of
738 tropospheric aerosols inferred from a global three-dimensional simulation of ^{210}Pb , *J. Geophys.*
739 *Res.*, *98(D11)*, 20,573-20,586.

740 Bey, I., D.J. Jacob, R.M. Yantosca, J.A. Logan, B. Field, A.M. Fiore, Q. Li, H. Liu, L.J.
741 Mickley, and M. Schultz (2001), Global modeling of tropospheric chemistry with assimilated
742 meteorology: Model description and evaluation, *J. Geophys. Res.*, *106*, 23,073-23,096.

743 Bloom, S., A. da Silva, D. Dee, M. Bosilovich, J.-D. Chern, S. Pawson, S. Schubert, M.
744 Sienkiewicz, I. Stajner, W.-W. Tan, and M.-L. Wu (2005). Documentation and Validation of
745 the Goddard Earth Observing System (GEOS) Data Assimilation System - Version 4.
746 *Technical Report Series on Global Modeling and Data Assimilation* (Editor Max J. Suarez),
747 NASA/TM-2005-104606, Vol. 26, NASA Goddard Space Flight Center, Greenbelt, Maryland,
748 April 2005.

749 Bourles, D.L. (1992), Beryllium isotopes in the Earth's environment, in *Encyclopedia of Earth*
750 *System Science* (Editor-in-Chief, W.A. Nierenberg), Vol. 1, 337-352, Academic Press, Inc.,
751 Harcourt Brace Jovanovich, Publishers.

752 Brost, R.A., J. Feichter, and M. Heimann (1991), Three-dimensional simulation of ^7Be in a
753 global climate model, *J. Geophys. Res.*, *96(D12)*, 22,423-22,445.

754 Collins, W.J., R.G. Derwent, B. Garnier, C.E. Johnson, and M.G. Sanderson, and D.S. Stevenson
755 (2003), Effect of stratosphere-troposphere exchange on the future tropospheric ozone trend, *J.*
756 *Geophys. Res.*, *108(D12)*, 8528, doi:10.1029/2002JD002617.

757 Considine, D.B., D.J. Bergmann, and H. Liu (2005), Sensitivity of Global Modeling Initiative
758 chemistry and transport model simulations of radon-222 and lead-210 to input meteorological
759 data, *Atmos. Chem. Phys.*, 5, 3389-3406.

760 Considine, D.B., J.A. Logan, and M.A. Olsen (2008), Evaluation of near-tropopause ozone
761 distributions in the Global Modeling Initiative combined stratosphere/troposphere model with
762 ozonesonde data, *Atmos. Chem. Phys.*, 8, 2365-2385.

763 Cristofanelli, P., et al. [2003], Stratosphere-to-troposphere transport: A model and method
764 evaluation, *J. Geophys. Res.*, 108(D12), 8525, doi:10.1029/2002JD002600.

765 Dibb, J. E., R. W. Talbot, and G. L. Gregory (1992), Beryllium 7 and Lead 210 in the Western
766 Hemisphere Arctic Atmosphere: Observations From Three Recent Aircraft-Based Sampling
767 Programs, *J. Geophys. Res.*, 97(D15), 16,709–16,715.

768 Dibb, J. E., L. D. Meeker, R. C. Finkel, J. R. Southon, M. W. Caffee, and L. A. Barrie (1994),
769 Estimation of stratospheric input to the Arctic troposphere: ⁷Be and ¹⁰Be in aerosols at Alert,
770 Canada, *J. Geophys. Res.*, 99(D6), 12,855–12,864.

771 Dibb, J., R. Talbot, K. Klemm, G. Gregory, H. Singh, J. Bradshaw, and S. Sandholm (1996),
772 Asian influence over the western North Pacific during the fall season: Inferences from lead
773 210, soluble ionic species and ozone, *J. Geophys. Res.*, 101(D1), 1779-1792.

774 Dibb, J. E., R. W. Talbot, B. L. Lefer, E. Scheuer, G. L. Gregory, E. V. Browell, J. D. Bradshaw,
775 S. T. Sandholm, and H. B. Singh (1997), Distributions of beryllium 7 and lead 210, and soluble
776 aerosol-associated ionic species over the western Pacific: PEM West B, February–March 1994,
777 *J. Geophys. Res.*, 102(D23), 28,287–28,302.

778 Dobb, J. E., R. W. Talbot, E. M. Scheuer, D. R. Blake, N. J. Blake, G. L. Gregory, G. W. Sachse,
779 and D. C. Thornton (1999), Aerosol chemical composition and distribution during the Pacific
780 Exploratory Mission (PEM) Tropics, *J. Geophys. Res.*, *104(D5)*, 5785–5800.

781 Dobb, J. E., R. W. Talbot, and E. M. Scheuer (2000), Composition and distribution of aerosols
782 over the North Atlantic during the Subsonic Assessment Ozone and Nitrogen Oxide
783 Experiment (SONEX), *J. Geophys. Res.*, *105(D3)*, 3709–3717.

784 Dobb, J. E., R. W. Talbot, E. M. Scheuer, G. Seid, M. A. Avery, and H. B. Singh (2003), Aerosol
785 chemical composition in Asian continental outflow during the TRACE-P campaign:
786 Comparison with PEM-West B, *J. Geophys. Res.*, *108(D21)*, 8815,
787 doi:10.1029/2002JD003111.

788 Dobb, J. E., R. W. Talbot, E. Scheuer, G. Seid, L. DeBell, B. Lefer, and B. Ridley (2003),
789 Stratospheric influence on the northern North American free troposphere during TOPSE: ⁷Be
790 as a stratospheric tracer, *J. Geophys. Res.*, *108(D4)*, 8363, doi:10.1029/2001JD001347.

791 ?Dobb, J.E., E. Scheur, R. Talbot, M. Avery (2008), Stratospheric Influence on the Composition
792 of the Mid- and Upper-Troposphere over North America sampled by the NASA DC-8 during
793 INTEX A, (2006), *J. Geophys. Res.*, in press(?).

794 Dobb, J.E. (2007), Vertical mixing above Summit, Greenland: Insights into seasonal and high
795 frequency variability from the radionuclide tracers Be-7 and Pb-210, *Atmos. Environ.*, *41(24)*,
796 5020-5030.

797 Douglass, A.R., M.J. Prather, T.M. Hall, S.E. Strahan, P.J. Rasch, L.C. Sparling, L. Coy, and
798 J.M. Rodriguez (1999), Choosing meteorological input for the global modeling initiative
799 assessment of high-speed aircraft, *J. Geophys. Res.*, *104(D22)*, 27,545-27,564.

800 Douglass, A.R., M.R. Schoeberl, R.B. Rood, and S. Pawson (2003), Evaluation of transport in
801 the lower tropical stratosphere in a global chemistry and transport model, *J. Geophys. Res.*,
802 *108(D9)*, 4259, doi:10.1029/2002JD002696.

803 Duncan, B.N., S.E. Strahan, and Y. Yoshida (2007), Model study of the cross-tropopause
804 transport of biomass burning pollution, *Atmos. Chem. Phys.*, *7*, 3713-3736.

805 Duncan, B., et al., The influence of European pollution on ozone in the Near East and northern
806 Africa, *Atmos. Chem. Phys.*, *8*, 2267-2283, 2008.

807 Dutkiewicz, V.A., and L. Husain (1979), Determination of stratospheric ozone at ground level
808 using ⁷Be/ozone ratios, *Geophys. Res. Lett.*, *6*, 171-174.

809 Dutkiewicz, V.A., and L. Husain (1985), Stratospheric and tropospheric components of ⁷Be in
810 surface air, *J. Geophys. Res.*, *90*, 5783-5788.

811 Feely, H.W., R.J. Larsen, and C.G. Sanderson (1989), Factors that cause seasonal variations in
812 beryllium-7 concentrations in surface air, *J. Environ. Radioactivity*, *9*, 223-249.

813 Feichter, J., R.A. Brost, and M. Heimann (1991), Three-dimensional modeling of the
814 concentration and deposition of ²¹⁰Pb aerosols, *J. Geophys. Res.*, *96*, 22,447-22,460.

815 Field, C.V., G.A. Schmidt, D. Koch, and C. Salyk (2006), Modeling production and climate-
816 related impacts on ¹⁰Be concentration in ice cores, *J. Geophys. Res.*, *111*, D15107,
817 doi:10.1029/2005JD006410.

818 Fiore, A.M., et al. (2009), Multimodel estimates of intercontinental source-receptor relationships
819 for ozone pollution, *J. Geophys. Res.*, *114*, D04301, doi:10.1029/2008JD010816.

820 Giorgi, F., and W.L. Chameides (1986), Rainout lifetimes of highly soluble aerosols and gases as
821 inferred from simulations with a general circulation model, *J. Geophys. Res.*, *91(D13)*, 14,367-
822 14,376.

823 Graustein, W.C., and K. K. Turekian (1996), ^7Be and ^{210}Pb indicate an upper tropospheric source
824 for elevated ozone in the summertime subtropical free troposphere of the eastern North
825 Atlantic, *Geophys. Res. Lett.*, *23*, 539-542.

826 Heikkila, U., J. Beer, and V. Alfimov (2008a), Beryllium-10 and beryllium-7 in precipitation in
827 Dubendorf (440 m) and at Jungfraujoch (3580 m), Switzerland (1998-2005), *J. Geophys. Res.*,
828 *113*, D11104, doi:10.1029/2007JD009160.

829 Heikkila, U., J. Beer, and J. Feichter (2008b), Modeling cosmogenic radionuclides ^{10}Be and ^7Be
830 during the Maunder Minimum using the ECHAM5-HAM general circulation model, *Atmos.*
831 *Chem. Phys.*, *8*, 2797-2809.

832 Helmig, D., S.J. Oltmans, T.O. Morse, and J.E. Dibb (2007), What is causing high ozone at
833 Summit, Greenland? *Atmos. Environ.*, *41*, 5031-5043.

834 Hirsch, R.M., and E.J. Gilroy (1984), Methods of fitting a straight line to data: Examples in
835 water resources, *Water Res. Bull.*, *20*, 705-711.

836 Holton, J. R., P. H. Haynes, M. E. McIntyre, A. R. Douglass, R. B. Rood, and L. Pfister (1995),
837 Stratosphere-Troposphere Exchange, *Rev. Geophys.*, *33*(4), 403-439.

838 Hsu, J., M.J. Prather, and O. Wild (2005), Diagnosing the stratosphere-to-troposphere flux of
839 ozone in a chemistry transport model, *J. Geophys. Res.*, *110*, D19305,
840 doi:10.1029/2005JD006045.

841 Hsu, J., and M.J. Prather (2009), Stratospheric variability and tropospheric ozone, *J. Geophys.*
842 *Res.*, *114*, D06102, doi:10.1029/2008JD010942.

843 Husain, L., P.E. Coffey, R.E. Meyers, and R.T. Cederwall (1977), Ozone transport from
844 stratosphere to troposphere, *Geophys. Res. Lett.*, *4*, 363-365.

845 Johnson, W.B., and W. Viezee (1981), Stratospheric ozone in the lower troposphere – I.
846 Presentation and interpretation of aircraft measurements, *Atmos. Environ.*, *15*, 1309-1323.

847 Jordan, C. E., J. E. Dibb, and R. C. Finkel (2003), $^{10}\text{Be}/^7\text{Be}$ tracer of atmospheric transport and
848 stratosphere-troposphere exchange, *J. Geophys. Res.*, *108*(D8), 4234,
849 doi:10.1029/2002JD002395.

850 Koch, D.M., D.J. Jacob, and W.C. Graustein (1996), Vertical transport of tropospheric aerosols
851 as indicated by ^7Be and ^{210}Pb in a chemical tracer model, *J. Geophys. Res.*, *101*, 18,651-
852 18,666.

853 Koch, D.M., and D. Rind (1998), Beryllium 10/beryllium 7 as a tracer of stratospheric transport,
854 *J. Geophys. Res.*, *103*(D4), 3907-3917.

855 Koch, D., G. A. Schmidt, and C. V. Field (2006), Sulfur, sea salt, and radionuclide aerosols in
856 GISS ModelE, *J. Geophys. Res.*, *111*, D06206, doi:10.1029/2004JD005550.

857 Kritz, M.A., S.W. Rosner, E.F. Danielsen, and H.B. Selkirk (1991), Air mass origins and
858 troposphere-to-stratosphere exchanges associated with mid-latitude cyclogenesis and
859 tropopause folding inferred from ^7Be measurements, *J. Geophys. Res.*, *96*, 17,405-17,414.

860 Lal, D., and B. Peters (1967), Cosmic ray produced radioactivity on the Earth, in *Handuch der*
861 *Physik*, *46/2*, edited by K. Sitte, pp.551-612, Springer-Verlag, New York.

862 Li, Q., D.J. Jacob, T.D. Fairlie, H. Liu, R.V. Martin, and R.M. Yantosca (2002), Stratospheric
863 versus pollution influences on ozone at Bermuda: Reconciling past analyses, *J. Geophys. Res.*,
864 *107*(D22), 4611, doi:10.1029/2002JD002138.

865 Liang, Q., A.R. Douglass, B.N. Duncan, R.S. Stolarski, and J.C. Witte (2009), The governing
866 processes and timescales of stratosphere-to-troposphere transport and its contribution to ozone
867 in the Arctic troposphere, *Atmos. Chem. Phys.*, *9*, 3011-3025.

868 Lin, S.-J. (2004), A “vertically Lagrangian” finite-volume dynamical core for global models,
869 *Mon. Wea. Rev.*, *132*, 2293-2307.

870 Liu, H., D.J. Jacob, I. Bey, and R.M. Yantosca (2001), Constraints from ^{210}Pb and ^7Be on wet
871 deposition and transport in a global three-dimensional chemical tracer model driven by
872 assimilated meteorological fields, *J. Geophys. Res.*, *106*, 12,109-12,128.

873 Liu, H., D. J. Jacob, J. E. Dibb, A. M. Fiore, and R. M. Yantosca (2004), Constraints on the
874 sources of tropospheric ozone from ^{210}Pb - ^7Be - O_3 correlations, *J. Geophys. Res.*, *109*, D07306,
875 doi:10.1029/2003JD003988.

876 Masarik, J., and J. Beer (1999), Simulation of particle fluxes and cosmogenic nuclide production
877 in the Earth’s atmosphere, *J. Geophys. Res.*, *104*, 12,099-12,111.

878 McLinden, C.A., S.C. Olsen, B. Hannegan, O. Wild, and M.J. Prather (2000), Stratospheric
879 ozone in 3-D models: A simple chemistry and the cross-tropopause flux, *J. Geophys. Res.*, *105*,
880 14,653-14,665.

881 Miller, R.L., and J.S. Kahn (1962), Statistical analysis in the geological sciences, p204-210, John
882 Wiley and Sons, New York, New York.

883 O’Brien, K., A. De La Zerda Lerner, M.A. Shea, and D.F. Smart (1991), The production of
884 cosmogenic isotopes in the Earth’s atmosphere and their inventories, in *The Sun in Time*,
885 pp.317-342, Univ. of Ariz. Press, Tucson.

886 Olsen, M.A., M.R. Schoeberl, and A.R. Douglass (2004), Stratosphere-troposphere exchange of
887 mass and ozone, *J. Geophys. Res.*, *109*, D24114, doi:10.1029/2004JD005186.

888 Pawson, S., et al. (2008), Goddard Earth Observing System chemistry-climate model simulations
889 of stratospheric ozone-temperature coupling between 1950 and 2005, *J. Geophys. Res.*, in
890 press.

891 Prather, M., and D. Ehhalt (2001), Atmospheric chemistry and greenhouse gases, in *Climate*
892 *Change 2001: The Scientific Basis*, edited by J.T. Houghton et al., pp.239-287, Cambridge
893 Univ. Press, New York.

894 Prospero, J.M., et al. (1995), Temporal variability of summer-time ozone and aerosols in the free
895 troposphere over the eastern North Atlantic, *Geophys. Res. Lett.*, *22*, 2925-2928.

896 Raisbeck, G.M., et al. (1981), Cosmogenic Be-10/Be-7 as a probe for atmospheric transport
897 processes, *Geophys. Res. Lett.*, *8*, 1015-1018.

898 Rangarajan, C., and S. Gopalakrishnan (1970), Seasonal variation of beryllium-7 relative to
899 caesium-137 in surface air at tropical and sub-tropical latitudes, *Tellus*, *22*, 115-120.

900 Rehfeld, S. and M. Heimann (1995), Three dimensional atmospheric transport simulation of the
901 radioactive tracers ^{210}Pb , ^7Be , ^{10}Be , and ^{90}Sr , *J. Geophys. Res.*, *100*(D12), 26,141-26,161.

902 Rind, D., and J. Lerner (1996), Use of on-line tracers as a diagnostic tool in general circulation
903 model development, 1. Horizontal and vertical transport in the troposphere, *J. Geophys. Res.*,
904 *101*(D7), 12,667-12,683.

905 Rind, D., J. Lerner, J. Jonas, and C. McLinden (2007), Effects of resolution and model physics
906 on tracer transports in the NASA Goddard Institute for Space Studies general circulation
907 models, *J. Geophys. Res.*, *112*, D09315, doi:10.1029/2006JD007476.

908 Rotman, D.A., et al. (2001), Global Modeling Initiative assessment model: Model description,
909 integration, and testing of the transport shell, *J. Geophys. Res.*, *106*, 1669-1691.

910 Sanak, J., G. Lambert, and B. Ardouin (1985), Measurements of stratosphere-troposphere
911 exchange in Antarctica by using short-lived cosmonuclides, *Tellus, Ser. B*, *37*, 109-115.

912 Schoeberl, M.R., A.R. Douglass, Z. Zhu, and S. Pawson (2003), A comparison of the lower
913 stratospheric age spectra derived from a general circulation model and two data assimilation
914 systems, *J. Geophys. Res.*, *108(D3)*, 4113, doi:10.1029/2002JD002652.

915 Schoeberl, M.R. (2004), Extratropical stratosphere-troposphere mass exchange, *J. Geophys. Res.*,
916 *109*, D13303, doi:10.1029/2004JD004525.

917 Shindell, D.T., G. Faluvegi, and N. Bell (2003), Preindustrial-to-present-day radiative forcing by
918 tropospheric ozone from improved simulations with the GISS chemistry-climate GCM, *Atmos.*
919 *Chem. Phys.*, *3*, 1675-1702.

920 Stajner, I., et al. (2008), Assimilated ozone from EOS-Aura: Evaluation of the tropopause region
921 and tropospheric columns, *J. Geophys. Res.*, *113*, D16S32, doi:10.1029/2007JD008863.

922 Stevenson, D.S., et al. (2006), Multimodel ensemble simulations of present-day and near-future
923 tropospheric ozone, *J. Geophys. Res.*, *111*, D08301, doi:10.1029/2005JD006338.

924 Stohl, A., et al., (2003), Stratosphere-troposphere exchange: A review, and what we have learnt
925 from STACCATO, *J. Geophys. Res.*, *108(D12)*, 8516, doi:10.1029/2002JD002490.

926 Strahan, S.E., and A.R. Douglass (2004), Evaluating the credibility of transport processes in
927 simulations of ozone recovery using the Global Modeling Initiative three-dimensional model,
928 *J. Geophys. Res.*, D05110, doi:10.1029/2003JD004238.

929 Strahan, S.E., B.N. Duncan, and P. Hoor (2007), Observationally-derived diagnostics of
930 transport in the lowermost stratosphere and their application to the GMI chemistry transport
931 model, *Atmos. Chem. Phys.*, *7*, 2435-2445.

932 Strahan, S.E., M.R. Schoeberl, and S.D. Steenrod (2009), The impact of tropical recirculation on
933 polar composition, *Atmos. Chem. Phys.*, *9*, 2471-2480.

934 Tanaka, N., and K.K. Turekian (1995), Determination of the dry deposition flux of SO₂ using
935 cosmogenic ³⁵S and ⁷Be measurements, *J. Geophys. Res.*, *100*, 2841-2848.

936 Terao, Y., J.A. Logan, A.R. Douglass, and R.S. Stolarski (2008), Contribution of stratospheric
937 ozone to the interannual variability of tropospheric ozone in the northern extratropics, *J.*
938 *Geophys. Res.*, *113*, D18309, doi:10.1029/2008JD009854.

939 Tsutsumi, Y., Y. Igarashi, Y. Zaizen, and Y. Makino (1998), Case studies of tropospheric ozone
940 events observed at the summit of Mount Fuji, *J. Geophys. Res.*, *103*, 16,935-16,951.

941 Usoskin, I. G., and G. A. Kovaltsov (2008), Production of cosmogenic ⁷Be isotope in the
942 atmosphere: Full 3-D modeling, *J. Geophys. Res.*, *113*, D12107, doi:10.1029/2007JD009725.

943 van Noije, T. P. C., H. J. Eskes, M. van Weele, and P. F. J. van Velthoven (2004), Implications
944 of the enhanced Brewer-Dobson circulation in European Centre for Medium-Range Weather
945 Forecasts reanalysis ERA-40 for the stratosphere-troposphere exchange of ozone in global
946 chemistry transport models, *J. Geophys. Res.*, *109*, D19308, doi:10.1029/2004JD004586.

947 Viezee, W., and H. B. Singh (1980), The distribution of beryllium-7 in the troposphere:
948 Implications on stratosphere/tropospheric air exchange, *Geophys. Res. Lett.*, *7*, 805-808.

949 Yang, Q., D.M. Cunnold, Y. Choi, Y. Wang, J. Nam, H.-J. Wang, L. Froidevaux, A.M.
950 Thompson, and P.K. Bhartia (2010), A study of tropospheric ozone column enhancements over
951 North America using satellite data and a global chemical transport model, *J. Geophys. Res.*,
952 *115*, D08302, doi:10.1029/2009JD012616.

953 Zanis, P., et al., (2003), An estimate of the impact of stratosphere-to-troposphere transport (STT)
954 on the lower free tropospheric ozone over the Alps using ¹⁰Be and ⁷Be measurements, *J.*
955 *Geophys. Res.*, *108*(D12), 8520, doi:10.1029/2002JD002604.

956 Ziemke, J. R., S. Chandra, B. N. Duncan, L. Froidevaux, P. K. Bhartia, P. F. Levelt, and J. W.
957 Waters (2006), Tropospheric ozone determined from Aura OMI and MLS: Evaluation of
958 measurements and comparison with the Global Modeling Initiative's Chemical Transport
959 Model, *J. Geophys. Res.*, *111*, D19303, doi:10.1029/2006JD007089.
960

961

962

963

964

Table 1. Characteristics of meteorological data sets used to drive the GMI CTM.

965

Data Set	Number of levels	Top Pressure (hPa)	Vertical Coordinate	Interface Pressure (hPa) ^a	Near-Tropopause Resolution (km)	Bottom layer depth (hPa, m)	Update Period (h)
GEOS1-STRAT	46	0.1	σ	N/A	~1.0	~12.13hPa, ~100m	6
GISS II'	23	0.002	σ -P	150	~1.8-2.5	~24.46hPa, ~200m	3
fvGCM	42 (55 ^b)	0.9 (0.01 ^b)	σ -P	200	~1.0	~14.89hPa, ~130m	3
GEOS-4	42 (55 ^b)	0.9 (0.01 ^b)	σ -P	200	~1.0	~14.89hPa, ~130m	3

966 ^aThe hybrid vertical coordinate consists of sigma (σ) levels below the interface pressure and

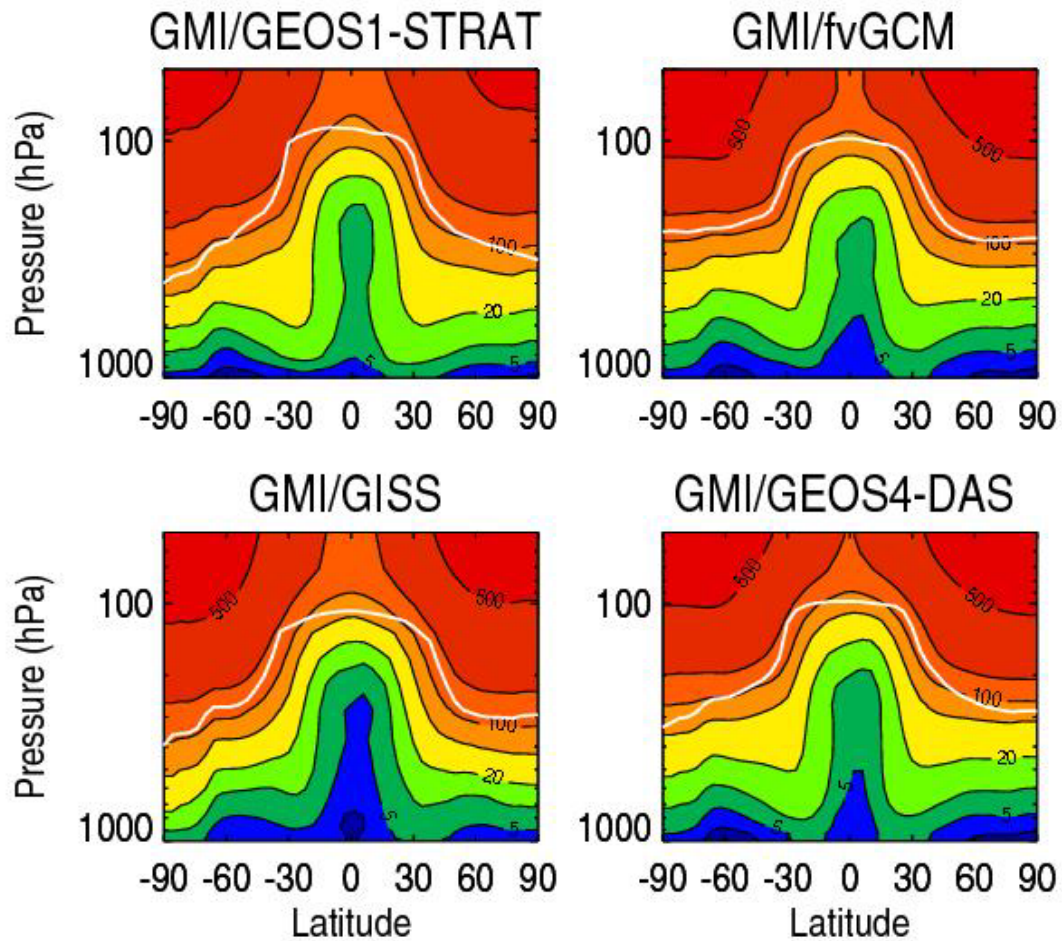
967 constant pressure (P) levels above.

968 ^bThe total number of vertical levels and top level pressure in the original meteorological data set.

969

970

971



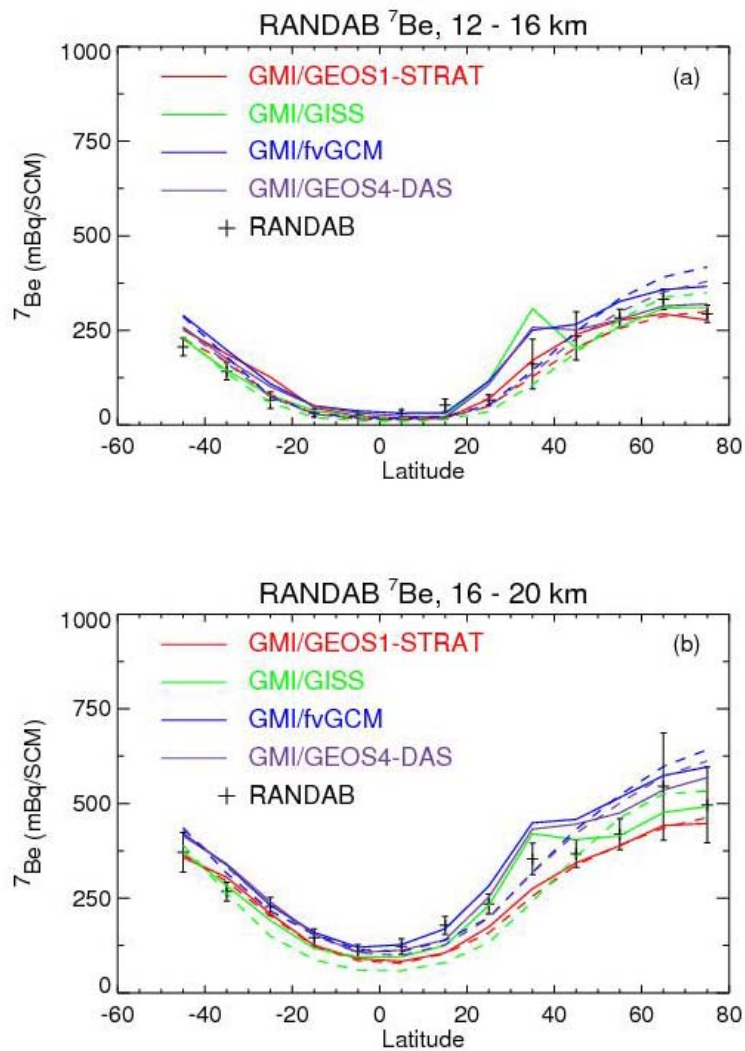
972

973 **Figure 1.** Annual zonal mean mixing ratios (mBq/SCM) of ⁷Be as a function of latitude and
974 pressure, as simulated by the standard GMI CTM. The white lines indicate the annual average
975 thermal tropopause height. Contour levels are 2, 5, 10, 20, 50, 100, 200, 500 mBq/SCM.

976

977

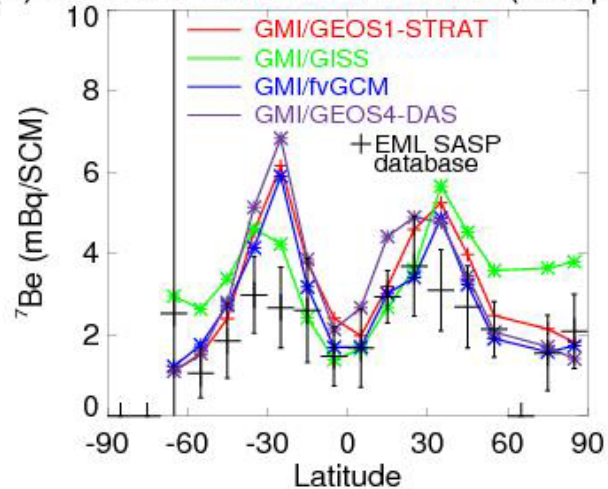
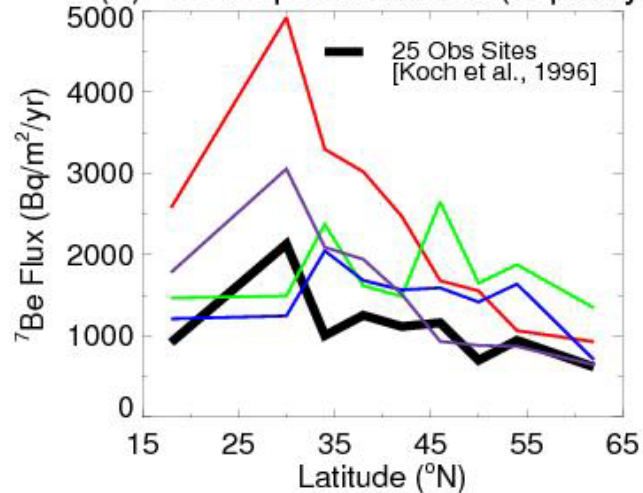
978



979

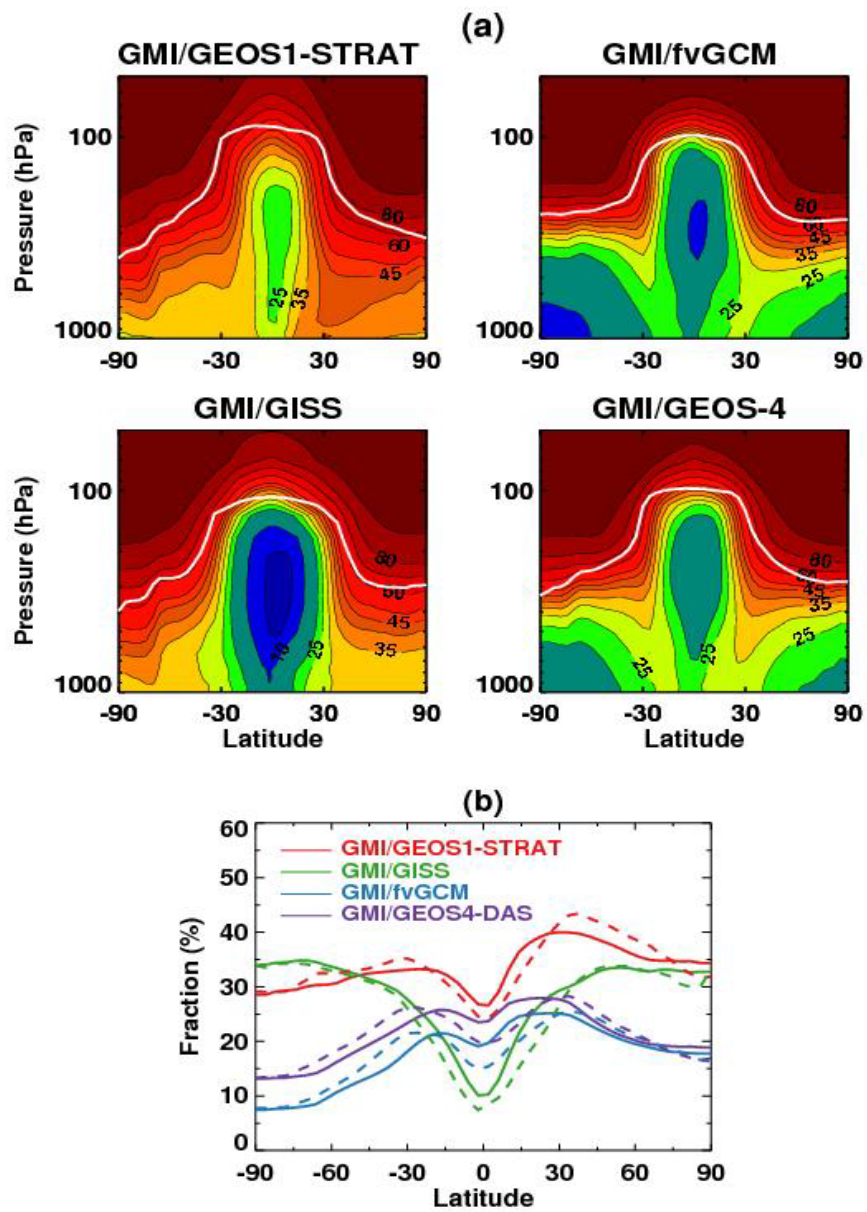
980 **Figure 2.** Observed and simulated latitudinal distributions of ^7Be in the (a) 12-16km and (b) 16-
981 20km regions. Observed data from the EML RANDAB database are averaged into 10° bins,
982 following Considine et al. [2005]. Error bars represent ± 2 times the standard error of the
983 averages. Model results are sampled at observation locations and month. Also shown as dashed
984 lines are model zonal mean ^7Be concentrations to show the global representativeness of the
985 averages constructed from sampling the simulations at the observation locations.

986

(a) Surface ^7Be Concentration (mBq/SCM)(b) ^7Be Deposition Flux ($\text{Bq}/\text{m}^2/\text{yr}$)

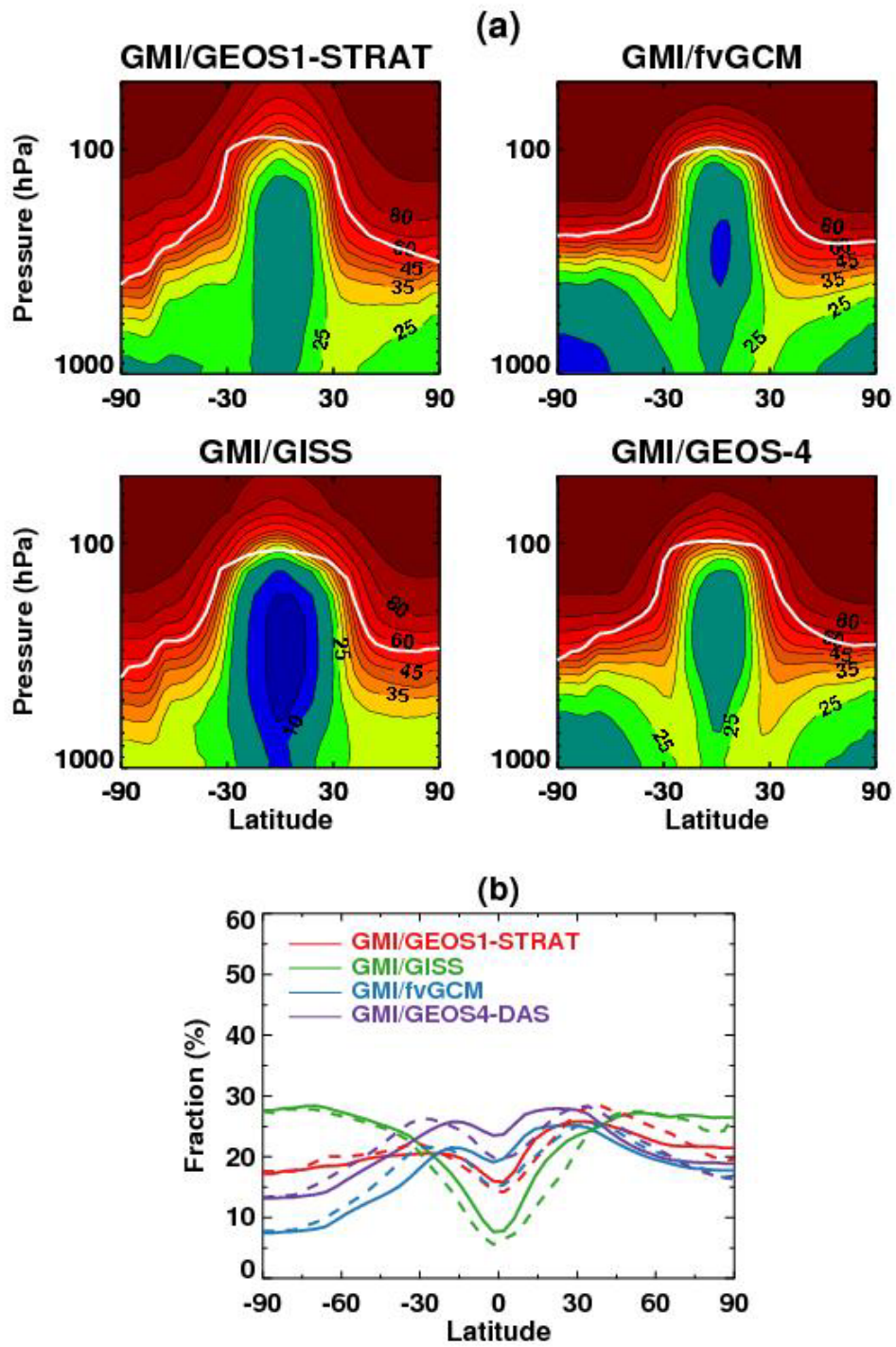
988

989 **Figure 3.** (a). Observed and simulated latitudinal distributions of ^7Be near the surface. ^7Be cross-
 990 tropopause fluxes were not adjusted for the GEOS1-STRAT, GISS and GEOS4-DAS
 991 simulations (see section 3). Observed data from the EML Surface Air Sampling Program (SASP)
 992 database are averaged into 10° bins. Those sites with elevation higher than 500m are not
 993 included. Error bars represent ± 2 times the standard error of the averages. Model results are
 994 sampled at observation locations and month. (b). Observed (black) and GMI simulated (color)
 995 annual average total deposition fluxes of ^7Be (at 25 sites) as a function of latitude. The data from
 996 individual sites are averaged over 4° latitude bins. The model is sampled at observation locations.
 997



999

1000 **Figure 4.** (a). Stratospheric fraction (%) of zonal mean tropospheric ^7Be concentrations in the
 1001 standard model simulations as a function of latitude and pressure. Values are annual averages.
 1002 The white lines indicate thermal tropopause height. Contour levels are 5, 10, 20, 25, 30, 35, 40,
 1003 45, 50, 60, 70, 80, 90%. (b). Stratospheric fraction of zonal mean surface ^7Be concentrations
 1004 (solid lines) and ^7Be total deposition fluxes (dashed lines) in the standard simulation. Values are
 1005 annual averages.

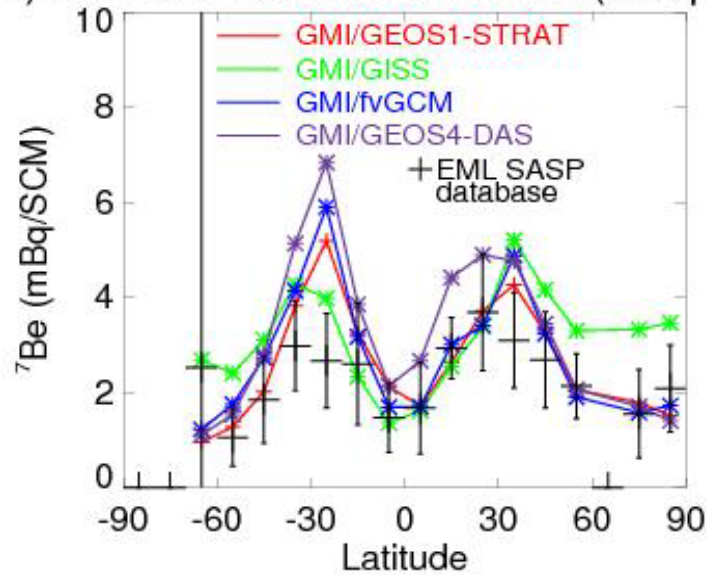


1008 **Figure 5.** Same as Figure 4, except that ^{7}Be cross-tropopause fluxes have been adjusted for

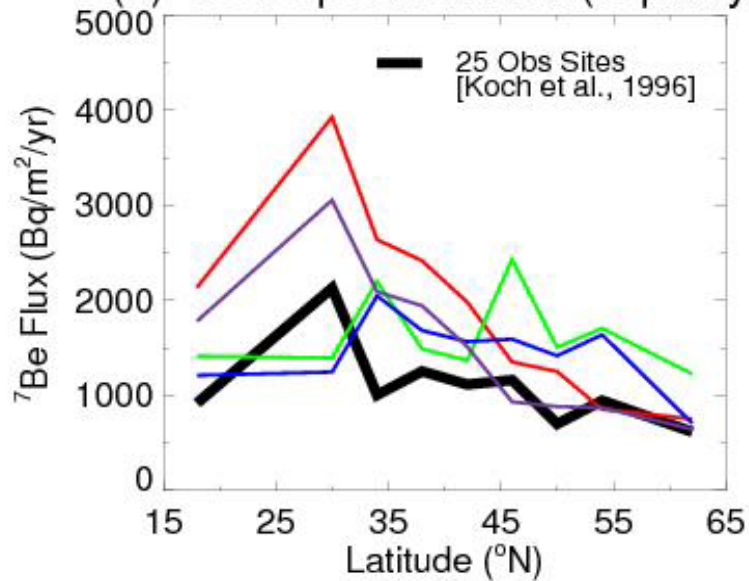
1009 GMI/GEOS1-STRAT and GMI/GISS.

1010

(a) Surface ^7Be Concentration (mBq/SCM)



(b) ^7Be Deposition Flux ($\text{Bq}/\text{m}^2/\text{yr}$)

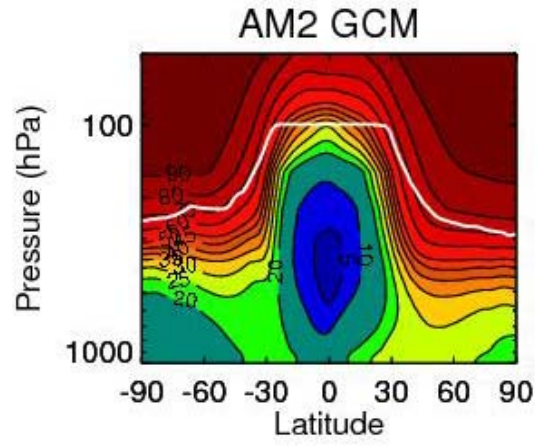


1011

1012 **Figure 6.** Same as Figure 3, except that ^7Be cross-tropopause fluxes have been adjusted for

1013 GMI/GEOS1-STRAT and GMI/GISS.

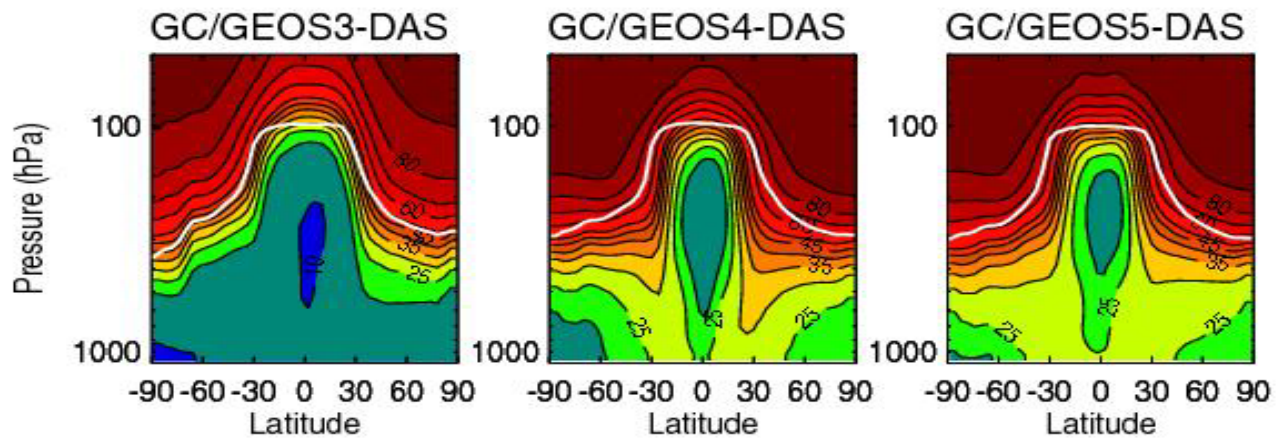
1014
1015
1016



1017
1018
1019

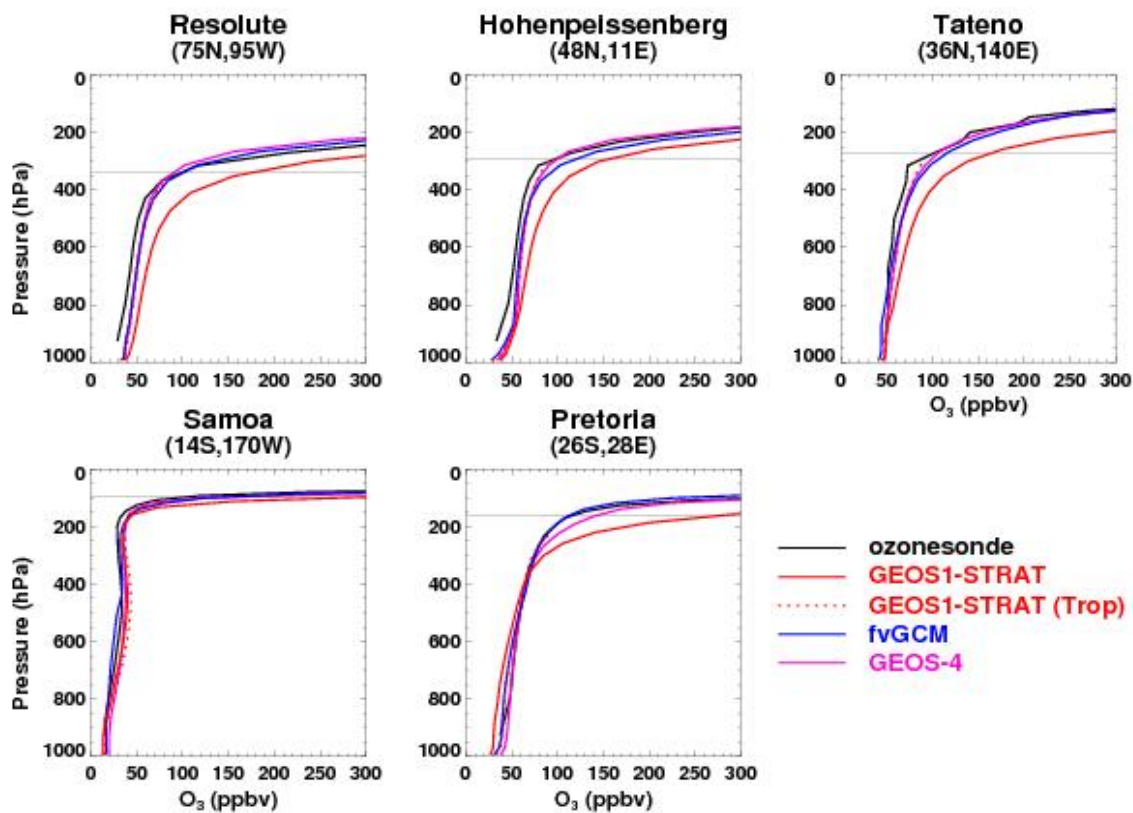
Figure 7. Same as Figure 4a, except for AM2 GCM.(year 1987).

1020
1021
1022
1023
1024
1025



1026
1027
1028
1029
1030
1031
1032
1033
1034
1035
1036
1037
1038

Figure 8. Same as Figure 4a, except that the GEOS-Chem model was driven with the GEOS3-DAS (2001), GEOS4-DAS (2004), and GEOS5-DAS (2004) meteorological fields.

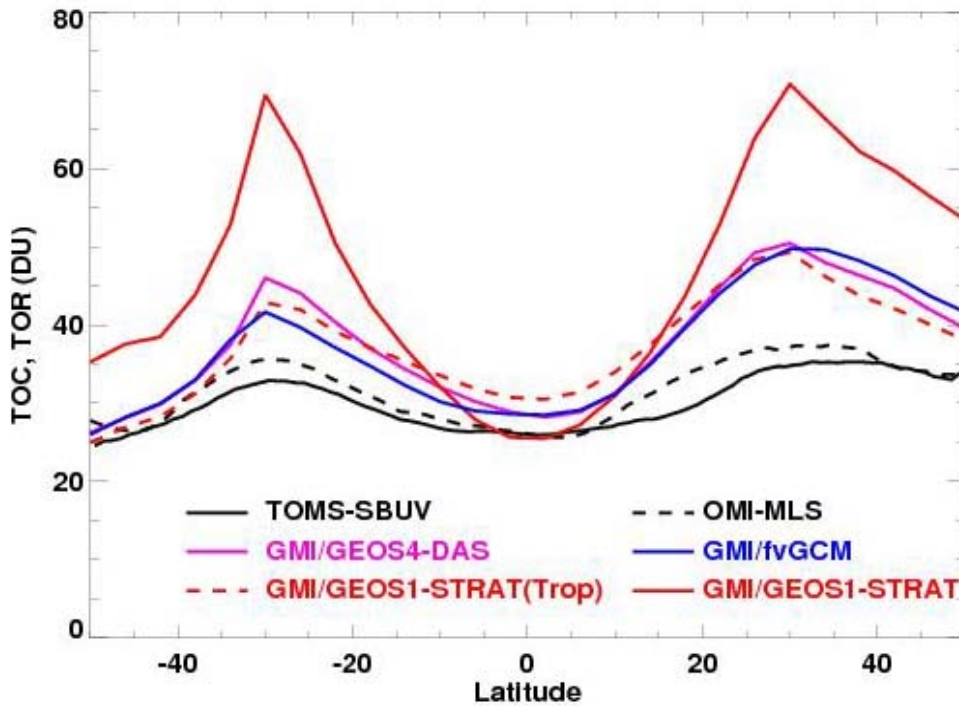


1039

1040 **Figure 9.** Comparisons of GMI simulated tropospheric ozone profiles (color lines) with
 1041 ozonesonde observations (black line) for a range of latitudes. Values are annual averages. Solid
 1042 color lines indicate the GMI Combo simulations. Also shown as dotted lines are tropospheric
 1043 ozone profiles as simulated by the GMI tropospheric model driven by the GEOS1-STRAT
 1044 meteorological field. The horizontal grey line indicates the approximate location of tropopause
 1045 (i.e., the pressure level corresponding to 100 ppbv ozone concentrations in the ozonesonde
 1046 observations).

1047

1048



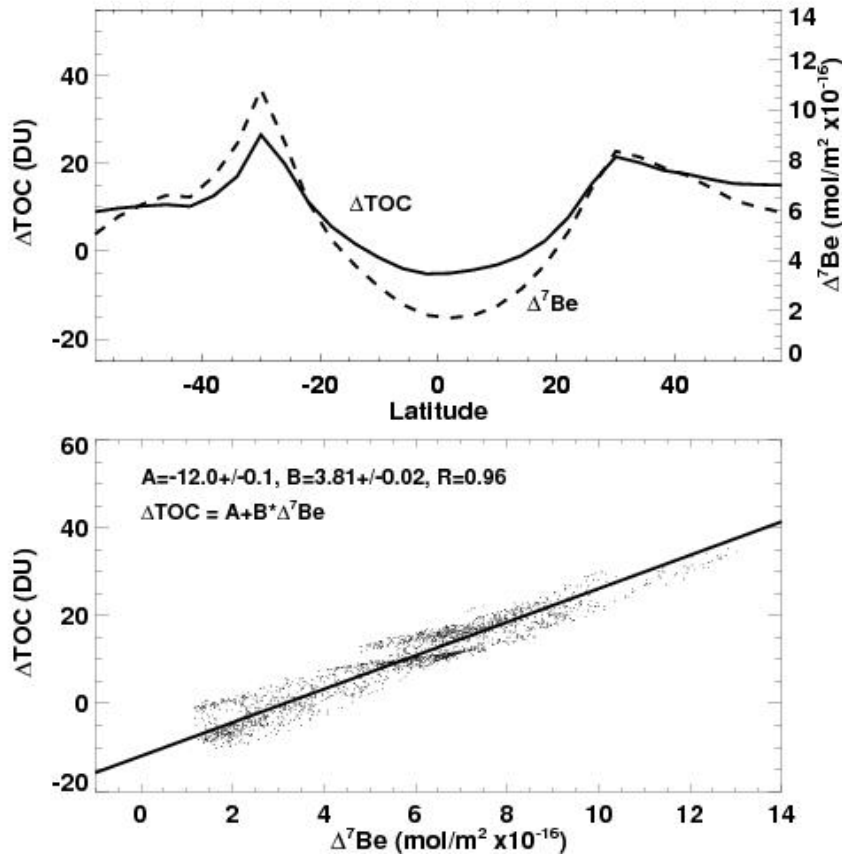
1049

1050 **Figure 10.** GMI Combo simulated annual zonal mean tropospheric ozone column (TOC in
1051 Dobson Units) compared with observed tropospheric ozone residuals (October 2004-July 2008
1052 average) from TOMS/SBUV and OMI/MLS. Also shown is the annual zonal mean TOC
1053 simulated by the tropospheric version of the GMI model.

1054

1055

1056



1057

1058

1059 **Figure 11.** (a). Latitudinal variations of annual zonal mean ^7Be overestimate ($\Delta^7\text{Be}$) and

1060 tropospheric ozone column overestimate (ΔTOC) as simulated by GMI/GEOS1-STRAT; (b). the

1061 correlation between the global distributions of $\Delta^7\text{Be}$ and ΔTOC . The lines of best fit are

1062 calculated using the reduced-major-axis (RMA) method [*Hirsch and Gilroy, 1984*]. See text for

1063 details.